The University of Alberta
Printing Department
Edmonton, Alberta

THE UNIVERSITY OF ALBERTA

RELEASE FORM

NAME OF AUTHOR: David G. Dickins

TITLE OF THESIS: Least-Squares Inverse Filtering of Seismic Reflection Data

DEGREE FOR WHICH THESIS WAS PRESENTED: M.Sc.

YEAR THIS DEGREE GRANTED: 1973

THE UNIVERSITY OF ALBERTA

LEAST-SQUARES INVERSE FILTERING OF SEISMIC REFLECTION DATA

by

© DAVID G. DICKINS

A THESIS

SUBMITTED TO THE FACULTY OF GRADUATE STUDIES AND RESEARCH

IN PARTIAL FULFILLMENT OF THE REQUIREMENTS FOR THE DEGREE

OF MASTER OF SCIENCE

IN

GEOPHYSICS

DEPARTMENT OF PHYSICS

EDMONTON, ALBERTA

FALL, 1973

THE UNIVERSITY OF ALBERTA

FACULTY OF GRADUATE STUDIES AND RESEARCH

The undersigned certify that they have read, and recommend to the Faculty of Graduate Studies and Research, for acceptance, a thesis entitled LEAST-SQUARES INVERSE FILTERING OF SEISMIC REFLECTION DATA submitted by David G. Dickins in partial fulfillment of the requirements for the degree of Master of Science in Geophysics.

ABSTRACT

A method for determining whether a wavelet is minimum-delay is evaluated; the method is used to show that the impulse response of the seismic recording instruments and seismometers used at the University of Alberta in 1971 is minimum-delay.

The transfer function of the seismic recording instruments and seismometers is used to generate the impulse response and the amplitude and phase spectra. A least-squares inverse to the impulse response is convolved with the seismic reflection data to produce instrument deconvolved data.

The method of least-squares predictive deconvolution is discussed. Single channel and multichannel predictive deconvolution methods are tested on some seismic reflection data and the results are compared. Both techniques seem about equally effective in resolving wave trains into approximations to reflection coefficient time series.

ACKNOWLEDGMENTS

I would like to thank Dr. G.L. Cumming for his encouragement and guidance during the course of this study.

Financial support for this research was provided by the Petroleum Aid to Education Fund.

Financial support for the writer was provided by a University of Alberta Graduate Teaching Assistantship.

Mrs. Mary Yiu did an excellent job of typing the manuscript.

TABLE OF CONTENTS

LIST OF FIGURES

CHAPTER 1

INTRODUCTION

1.1 Crustal Refraction and Reflection Studies

The crust, or outer layer of the earth, represents less than two percent of the earth's volume, yet it dominates man's view of the planet. Of primary importance as the source of economic wealth in the form of petroleum and mineral deposits, it has long been studied in an effort to locate such riches. As near surface deposits are discovered and exhausted, searchers must probe more deeply into the crust. The details of its structure as deduced by all geological and geophysical methods become increasingly more important. In addition, man studies the crust in an effort to predict such catastrophes as volcanoes and earthquakes and to minimize the damage they cause. Although such phenomena originate below the crust, we can only observe them through the crust, and we must know how the crust affects such indirect measurements.

The first indirect measurements of crustal structure were made using near earthquake observations. In 1910, a velocity discontinuity was discovered by Mohorovičić, and it has been defined as the base of the crust. It has been debated whether the discontinuity

represents a phase or a chemical transition. In 1925, a shallower velocity discontinuity was discovered by Conrad. It has been regarded as a non-universal transition from granitic to basic material.

The first field tests of the reflection seismic method applied to exploration were conducted in Oklahoma in 1921 (Schriever, 1952). The first recording of deep crustal reflections was made in Montana (Junger, 1951), where reflections were recorded in the time interval 7.0 to 8.5 seconds. Reports of deep crustal seismic reflections have been documented (Steinhart and Meyer, 1961). A good review of deep seismic sounding in northern Europe has been presented (Vogel, 1971). The American Geophysical Union series of geophysical monographs has periodically reviewed seismology (Steinhart and Smith, 1966; Knopoff, Drake, and Hart, 1968; Hart, 1969; Heacock, 1971).

A review of studies of crustal structure in Germany has been published (Dohr and Fuchs, 1967). A statistical study of deep reflections was done; histograms were plotted with reflection time versus number of reflections for a small region. It was found that reflections existed on the records in a statistical sense. The deep reflections were correlated only over short distances.

It has been suggested that the Mohorovičić discontinuity is stepwise, interrupted by a rhythmically arranged series of partial melts of lower velocity (Meisner, 1967). It has been shown that a simple layered model of the reflecting horizons is not consistent with the observed large amplitude and low cut-off frequency of deep reflections (Fuchs, 1969), but that a transition zone with a series of velocity reversals provides a satisfactory model.

The first seismic crustal study in Alberta was undertaken by a group of fifteen seismic parties (Richards and Walker, 1959). Measurements were recorded along a 130 kilometer reversed refraction profile, parallel to and 100 kilometers east of the frontal thrust of the Rocky Mountains. The depth to the Mohorovičić discontinuity was found to be 43 kilometers, with an upper mantle velocity of 8.2 kilometers per second. An intermediate discontinuity was found at a depth of 29 kilometers with a velocity of 7.2 kilometers per second below.

1.2 Crustal Studies at the University of Alberta

Explosion seismology was first used at the University of Alberta when a 250 kilometer east-west reversed refraction profile was shot in southern Alberta (Cumming, Garland, and Vozoff, 1962). A

crustal model was obtained which consisted of three layers between the basement and upper mantle. The refraction work was extended along two east-west reversed refraction profiles for 500 kilometers (Cumming and Kanasewich, 1966). In addition, a refraction profile extending west into the Rocky Mountains was shot.

The first deep reflection work at the University of Alberta was a study of near-vertical incidence seismic reflections at Lomond, Alberta (Kanasewich and Cumming, 1965). Good reflections were recorded at a time of 11.4 seconds along an expanding spread. The use of three-component geophone arrays showed that the event was near-vertical incidence. A T^2 versus X^2 analysis gave an average velocity from the top of the Mississippian to this reflector of 6.37 kilometers per second and a depth to the reflector of 34 kilometers. The discontinuity has been referred to locally as the Riel discontinuity to avoid implying that the Conrad is universal.

Seismic reflections were studied over four profiles for a total of 90 kilometers (Clowes, Kanasewich, and Cumming, 1968). Autopower spectral calculations showed that the energy of the reflected wavelets was concentrated in the five to fifteen Hertz range. Along

one profile, the Riel reflection was correlated over nearly 25 kilometers. Analysis of this data gave a revised average velocity of 6.2 kilometers per second to a depth of 34 kilometers.

The attenuation properties of the crust and the nature of the reflecting horizons were studied (Clowes and Kanasewich,1970). An attenuation model was obtained from a comparison of the data with synthetic seismograms which included attenuation as a function of frequency and depth. Autopower spectral analysis was used to examine the nature of the reflecting zones. It was concluded that models with first order discontinuities, linear gradients, and step-like velocity increases did not match the spectral characteristics of the reflections. A transition zone model consisting of sills of alternating high and low velocity material was in agreement with the observed data. The sills of the model were less than 0.2 kilometers thick extending over a zone less than 1 kilometer thick.

Studies of crustal structure in central Alberta were undertaken using P-codas from earthquake seismograms (Ellis and Basham, 1968). Vertical to radial spectral ratios were compared with theoretical ratios calculated using the Thomson-Haskell matrix formulation. With the aid of synthetic seismograms, an improved model

was obtained (Somerville and Ellis, 1972). Another crustal study in the same area was done using the P-coda spectral ratio method (Sprenke, 1972).

Synthetic seismogram calculations using asymptotic ray theory for plane-layered, homogeneous elastic media have been described (Hron and Kanasewich, 1971). Criteria for the selection of phases which make significant contributions to synthetic seismograms have been given (Hron, 1971). The synthetic seismogram calculations have been generalized to permit curvilinear interfaces in the media (Hron, personal communication).

A 760 kilometer refraction profile from Greenbush Lake, British Columbia to Swift Current, Saskatchewan was interpreted (Chandra and Cumming, 1972). A unified interpretation was found from an examination of previous refraction and reflection data and from gravity and magnetic surveys.

Investigation of an additional 40 kilometers of reflection data in southern Alberta has been undertaken (Cumming and Chandra, personal communication). The studies have used autopower spectral analysis and homomorphic deconvolution of the major reflecting zones of the deep crust in order to further define the details of the reflecting interfaces.

A seismic reflection crustal model has been obtained near Edmonton, Alberta (Ganley, 1973). Velocity analysis of a profile 13 kilometers long has indicated that fifteen degree southeasterly dips occur within the crust, with a total crustal thickness of 35.5 kilometers.

Homomorphic deconvolution has been used in analysis of earthquake seismograms (Alpaslan, personal communication).

Much of this work has indicated that deep crustal reflecting and refracting transitions are zones of alternating high and low velocities of less than 1 kilometer in extent, and the resolution of normal seismic records is insufficient to permit examination of the detail of these zones due to the overlap of pulses. Therefore, it was thought that it would be worthwhile to apply the techniques of deconvolution to reflection records from the deep crust in an effort to obtain more information about the structure of the transition zones.

CHAPTER 2

CONVOLUTION AND MINIMUM-DELAY

2.1 Introduction

Seismic reflection data is recorded in either analog or digital form. An analog trace is a continuous physical variable, while a digital trace is a discrete physical variable. A digital trace may be represented by a series of complex numbers which are samples or measurements of the physical variable at a constant time interval Δt. Thus, the trace X may be represented by the series $x_0, x_1, x_2, \ldots$ corresponding to samples of X at times 0, Δt, $2\Delta t$, ...

The mean of X is defined to be

$$\lim_{N\to\infty} \frac{1}{N} \sum_{j=0}^{N} x_j \quad . \tag{2.1}$$

The autocorrelation of X is defined to be

$$r_i = \sum_{j=0}^{\infty} x_{i+j} \bar{x}_j \quad , \tag{2.2}$$

where the horizontal bar means the complex conjugate. The trace E may be defined as white noise (Robinson, 1964). Then E must satisfy the following:

1. E must have zero mean;

2. the zero lag of the autocorrelation of E, r_0, must be finite; and

3. all other lags of the autocorrelation of E must be zero.

The seismic trace may be defined to be the convolution of white noise $e_0, e_1, e_2, \ldots$ with a characteristic wavelet $b_0, b_1, b_2, \ldots, b_n$ by the convolution equation

$$x_t = \sum_{s=0}^{\infty} b_s \, e_{t-s} \quad . \qquad 2.3$$

This equation may be written symbolically as

$$X = B*E \quad . \qquad 2.4$$

The object of deconvolution is to obtain E given X, since E represents the reflection coefficients of the earth beneath the seismic instruments - the reflection coefficients give details about the structure of the crust.

A two-length wavelet b_0, b_1 has a reverse $\bar{b}_1, \bar{b}_0$. The minimum-delay wavelet of the pair is the one in which the first sample is largest in magnitude; the other wavelet is maximum-delay. The convolution of minimum-delay wavelets gives a minimum-delay wavelet; the convolution of maximum-delay wavelets gives a

maximum-delay wavelet; and the convolution of one or more minimum-delay wavelets with one or more maximum-delay wavelets gives a mixed-delay wavelet.

2.2 Zeros of a Polynomial

The Z-transform of the wavelet $b_0, b_1, b_2, \ldots, b_n$ is a polynomial in z of order n,

$$b_0 + b_1 z + b_2 z^2 + \ldots + b_n z^n \quad . \qquad 2.5$$

If we factor this polynomial, we obtain it in the form

$$b_n (z-z_1)(z-z_2) \ldots (z-z_n) \quad . \qquad 2.6$$

The zeros of this polynomial are at $z = z_1, z_2, \ldots, z_n$. A two-length wavelet b_0, b_1 has a Z-transform $b_0 + b_1 z$ which can be factored to give $b_1[z-(-b_0/b_1)]$. The zero of this polynomial is at $z_1 = -b_0/b_1$. If the wavelet was minimum-delay, $|b_0| > |b_1|$, so $|z_1| > 1$. If the wavelet was maximum-delay, $|b_0| < |b_1|$, so $|z_1| < 1$. The boundary $|z| = 1$ separates minimum-delay zeros from maximum-delay zeros; this boundary is the unit circle in the complex z-plane. If we plot the zeros of a polynomial in the complex z-plane, we may determine whether the wavelet is minimum-delay or not.

Thus one method of determining whether a wavelet is minimum-delay or not is the factoring of the

polynomial obtained by Z-transforming the wavelet. If the wavelet is longer than a few samples, a general method of factorization is needed. Subroutines have been written to factor a polynomial; subroutine DPRQD from IBM's Scientific Subroutine Package was found to be the most satisfactory. DPRQD uses double-precision arrays, and it does not limit the order of the input polynomial. It provides an error return code which indicates any existing error condition. The subroutine takes considerably less than one minute of Central Processing Unit time on the IBM 360/67 at the University of Alberta Computing Center to factor a polynomial of order forty.

To test DPRQD a trial wavelet was chosen, the expansion of $(z+1.75)^{12}\ (z-1.1)^{2}$, which has been plotted in Figure 2.1. The resulting polynomial of order fourteen has a zero of order twelve at $z = -1.75$ and a zero of order two at $z = 1.1$. The zeros calculated by DPRQD have been plotted in the upper half of Figure 2.2. Note that only the upper half of the complex z-plane is plotted, since zeros occur singly on the real axis or as complex conjugate pairs symmetrical about the real axis. While the zeros show a large scatter, roughly on a circle centered at $z = -2.0$ with radius 1.0, it may

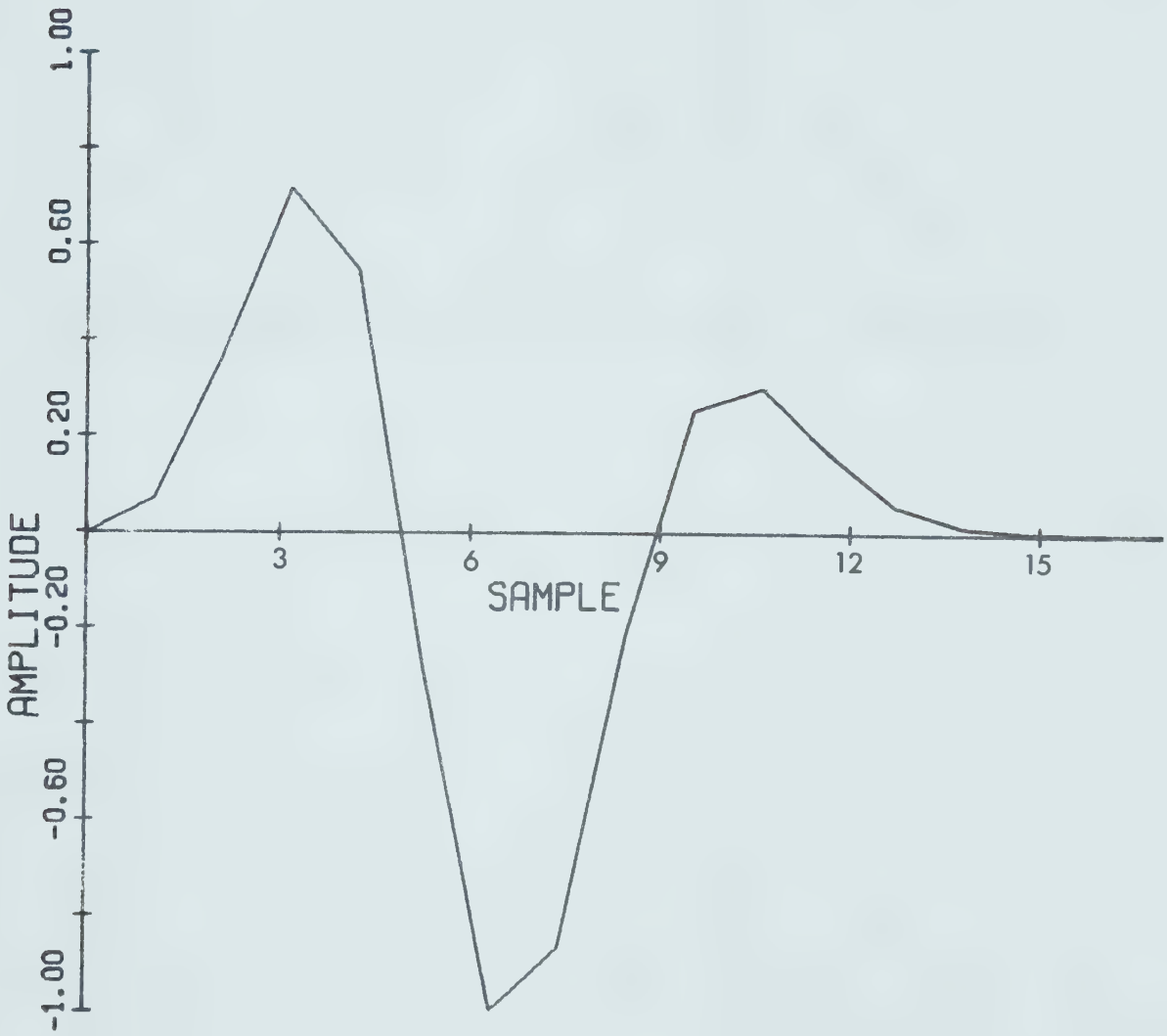

Figure 2.1. The trial wavelet.
Amplitude units are plotted versus sample units; the amplitude has been normalized to 1.0. The trial wavelet is minimum-delay.

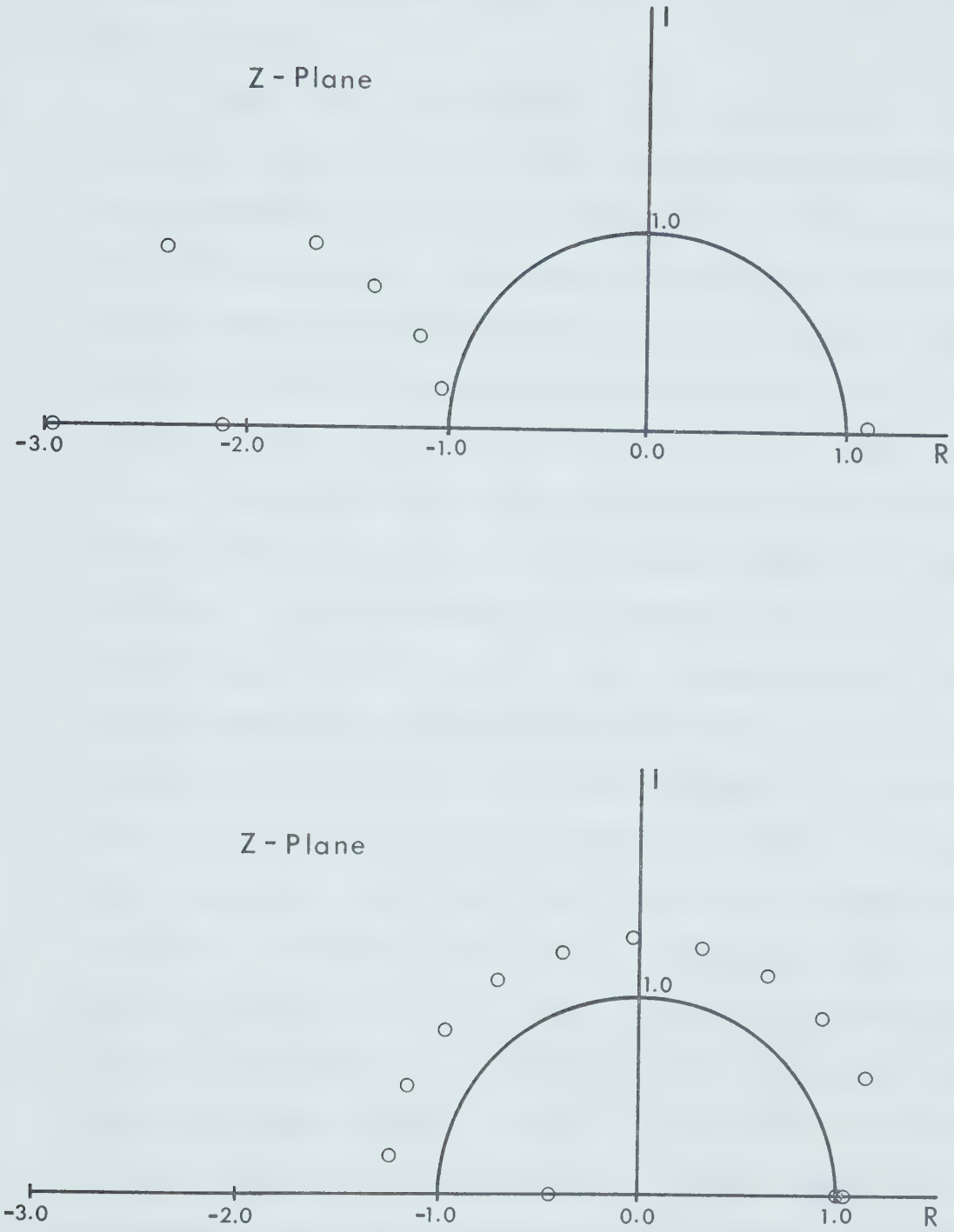

Figure 2.2. Zeros of the polynomials.
Upper diagram: zeros of the trial wavelet.
Lower diagram: zeros of the impulse response of the seismic recording instruments and seismometers used in 1971. In each case, only the upper half z-plane is plotted.

be noted that all the zeros are outside the unit circle as required.

DPRQD was also tested on a longer wavelet. The impulse response of the seismic recording instruments and seismometers used at the University of Alberta in 1971 was generated. The seismic recording instruments and seismometers are described in Chapter Three. The impulse response was sampled at an interval of Δt = 0.0056 seconds, and it has been plotted in Figure 2.3. It was truncated after twenty-four samples and Z-transformed; the polynomial of twenty-third order was input to DPRQD. The zeros of this polynomial have been plotted in the lower half of Figure 2.2. It may be seen that twenty zeros fall outside the unit circle, roughly on a circle centered at z = 0.0 with radius 1.2. Two other zeros fall on the unit circle where it crosses the positive real axis. The final zero falls on the negative real axis inside the unit circle. Since the mean of the samples was not removed, it may be suggested that removing the mean would put this zero on or outside the unit circle (O'Brien, 1969). It may be concluded that the impulse response is minimum-delay. This agrees with the conclusion drawn from examining the transfer function of the instruments and seismometers in the complex s-plane. The transfer function of the seismic recording instruments and seismometers is described in the Appendix.

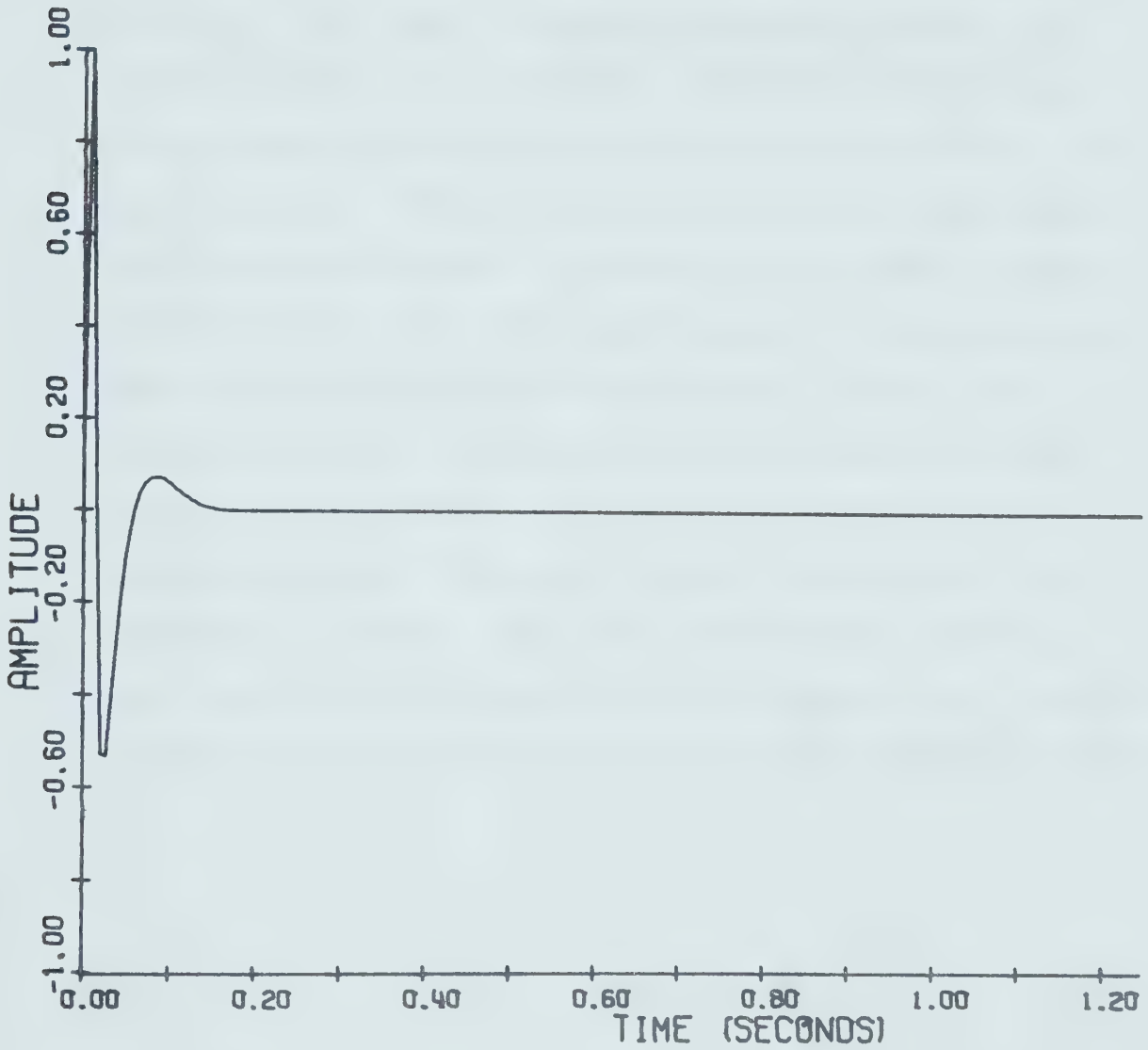

Figure 2.3. The impulse response of the seismic recording instruments and seismometers used at the University of Alberta in 1971. The sample interval Δt is 0.0056 seconds.

DPRQD has an error return code which indicates whether or not the expansion of the calculated zeros is identical to the input polynomial to six figures of accuracy. Although the calculated zeros of the trial wavelet satisfy this condition, they are not the same as the zeros which were originally used to generate the trial wavelet. Shorter wavelets, which were expressed exactly by six figures of accuracy, were input to DPRQD, and their zeros were recovered exactly. This indicates that the zeros calculated for the trial wavelet are correct, and that the reason they show scatter is that the trial wavelet must agree with the expansion of the calculated zeros to only six figures of accuracy. In conclusion, although the zeros found by this procedure show scatter, they appear to be sufficiently well resolved to indicate whether or not the polynomial is minimum-delay.

CHAPTER 3

INSTRUMENT DECONVOLUTION

3.1 Seismic Recording Instruments and Seismometers

In 1969, the University of Alberta seismic reflection equipment was deployed in two trucks; in each truck, one Texas Instruments VLF-2 amplifier system recorded six channels of data on a Precision Instruments seven track FM analog tape recorder. The s-plane representation of the seismic recording instruments is given in the Appendix. The impulse response of the seismic recording instruments is plotted in Figure 3.1, and the amplitude and phase spectra are plotted in the Appendix.

In 1970, the University of Alberta seismic reflection equipment was deployed in one truck, in which one Texas Instruments VLF-2 amplifier system recorded twelve channels of data on a Peripheral Equipment Corporation model 7830-9 digital tape recorder. The s-plane representation of the seismic recording instruments is given in the Appendix. The impulse response of the seismic recording instruments is plotted in Figure 3.2, and the amplitude and phase spectra are plotted in the Appendix.

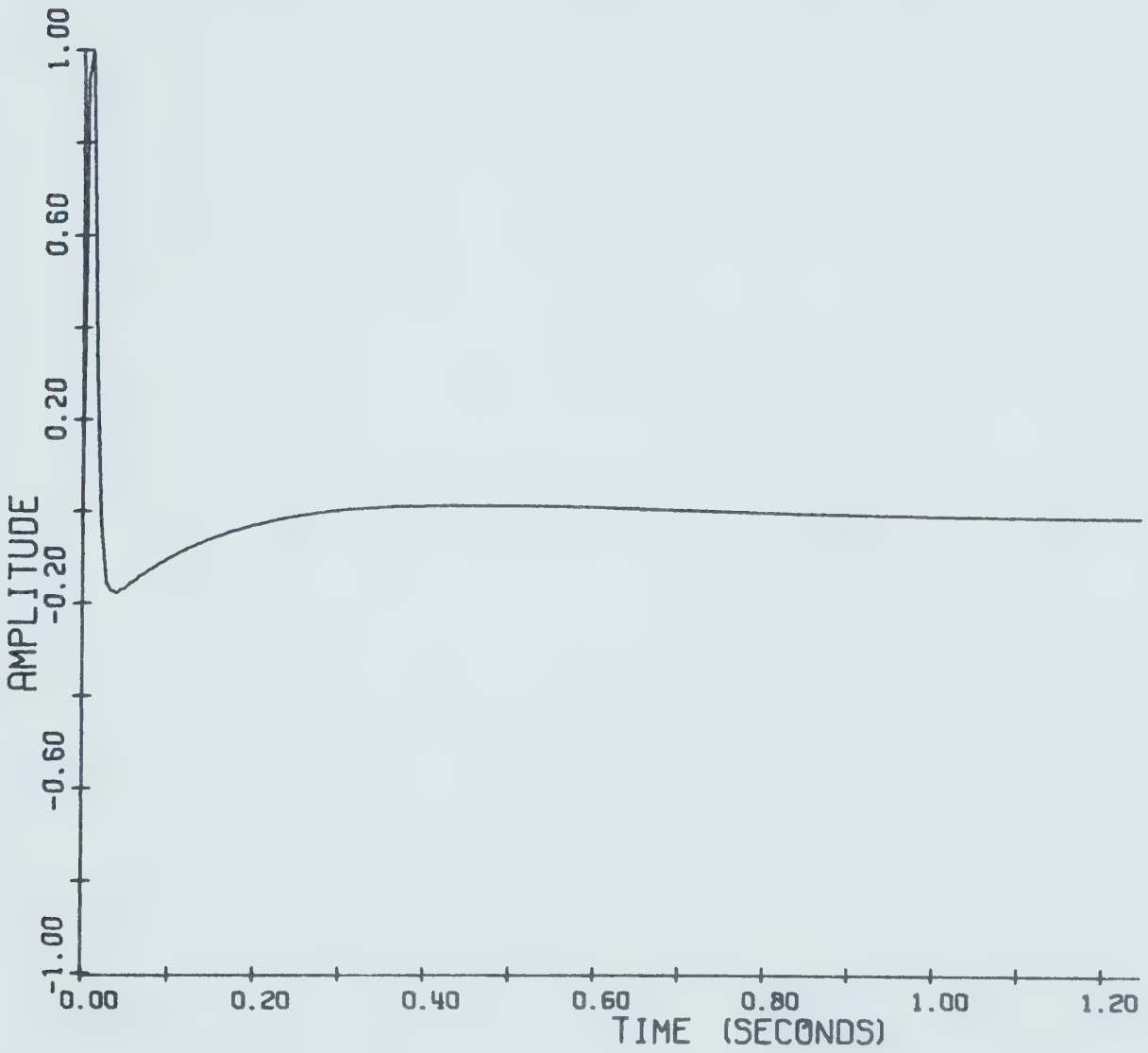

Figure 3.1. The impulse response of the seismic recording instruments used at the University of Alberta in 1969. The sample interval Δt is 0.0056 seconds.

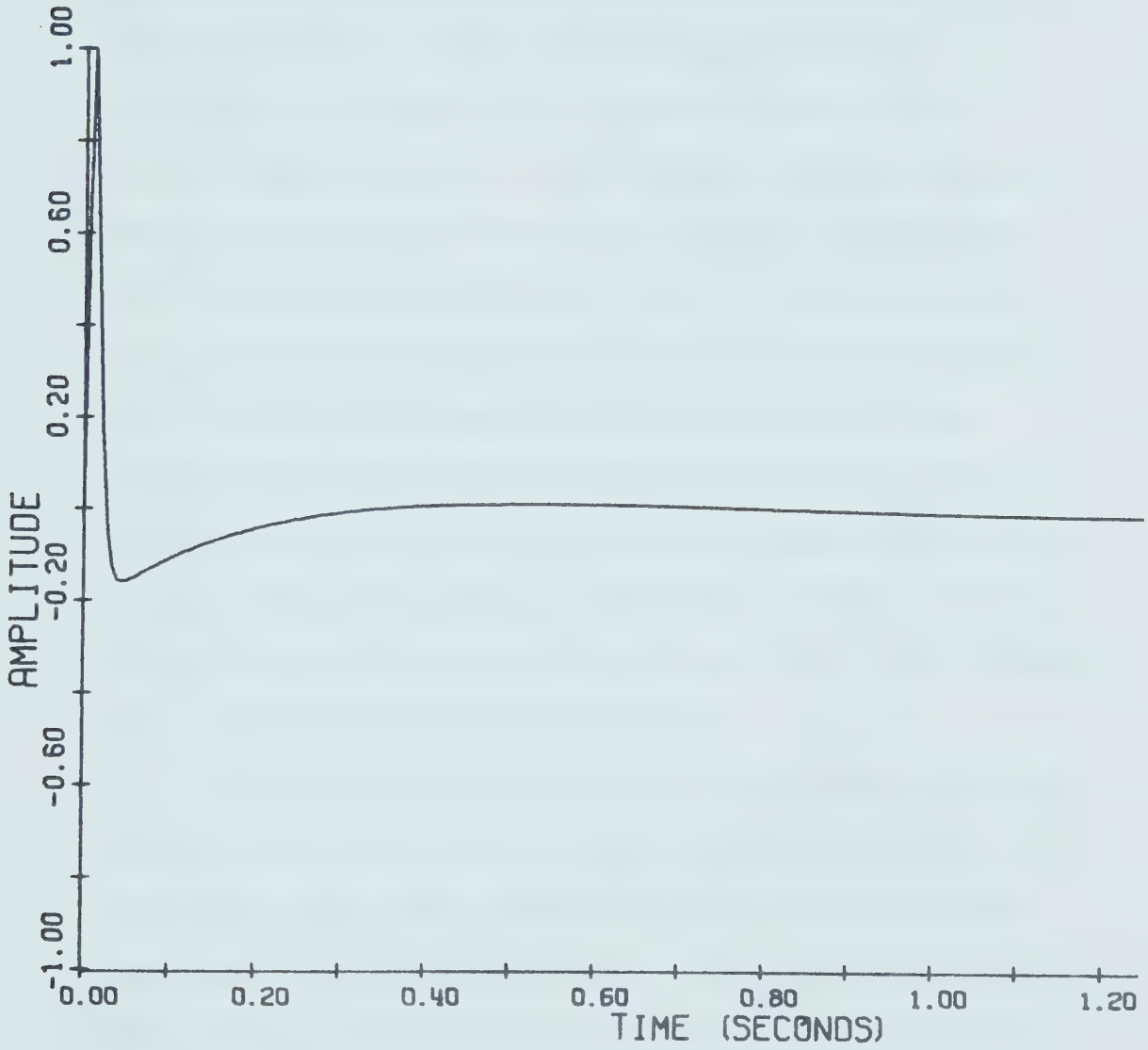

Figure 3.2. The impulse response of the seismic recording instruments used at the University of Alberta in 1970. The sample interval Δt is 0.0056 seconds.

In 1971, the University of Alberta seismic reflection equipment was deployed in one truck, in which one amplifier system (Alsopp, Burke, and Cumming, 1972) recorded twelve channels of data on a Peripheral Equipment Corporation model 7830-9 digital tape recorder. Each channel represented the output from a tapered array of sixteen Electro-Tech EVS-4 seismometers (Clowes, 1969). Two additional channels were recorded; one channel was shot instant from a radio receiver, and the other channel was absolute time from WWVB. These fourteen channels were recorded on a nine track synchronous tape recorder at a density of 800 bytes per inch with a tape velocity of 6.25 inches per second, resulting in a data transfer rate of 5000 bytes per second.

The signal was converted from analog to digital form by a converter with a resolution of thirteen bits plus sign providing a dynamic range of eighty-four decibels. Two eight-bit bytes were required to store each sample, so the sample rate was 2500 samples per second. Each channel was therefore sampled once every 14/2500 or 0.0056 seconds, and the Nyquist frequency was slightly above eighty-nine Hertz. The length of the records written was 4096 samples for a time interval of 22.94 seconds.

The multiplexer, analog to digital converter, and five thousand Hertz crystal clock plus associated interfaces and controls were contained in a modified model 120 Data Acquisition System manufactured by Datum Inc. Controls allowed the selection of from one to twenty channels to be sampled sequentially and the selection of record length up to a maximum of 4096 samples per channel.

The amplifier circuit had a flat response from one-tenth to fifty Hertz, and it consisted of an input transformer of eighteen decibels gain followed by a preamplifier of forty decibels gain connected to the amplifier by a two pole high pass Bessel filter which could be bypassed. The amplifier had switchable gain, and its output passed through a four pole low pass Bessel filter with a fifty Hertz corner.

The s-plane representation of the seismic recording instruments and seismometers used in 1971 is given in the Appendix. The impulse response of the seismic recording instruments and seismometers is plotted in Figure 2.3; the impulse response of the seismic recording instruments is plotted in Figure 3.3. The amplitude and phase spectra of the seismic recording instruments and of the seismic recording instruments and seismometers are plotted in the Appendix.

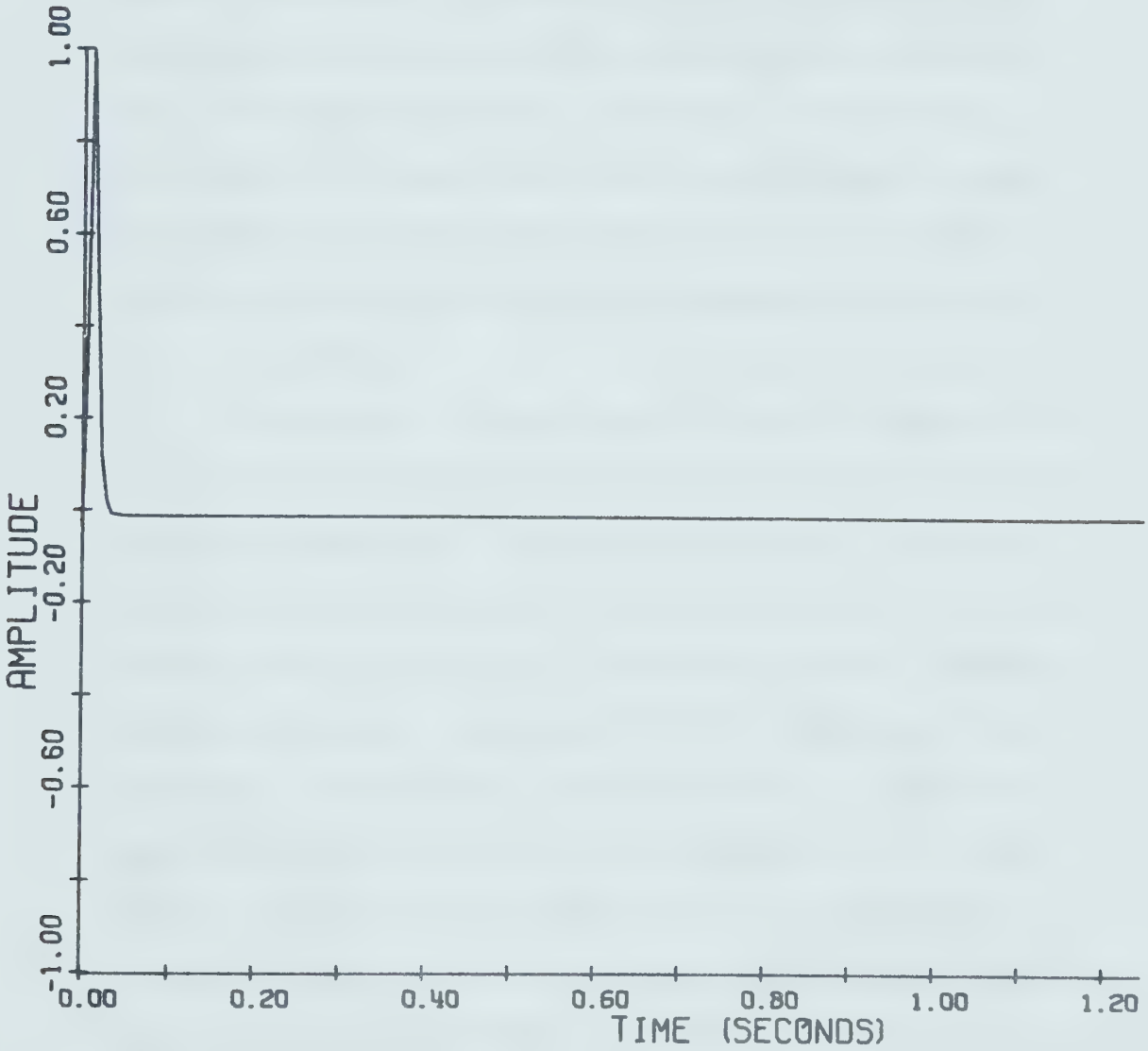

Figure 3.3. The impulse response of the seismic recording instruments used at the University of Alberta in 1971. The sample interval Δt is 0.0056 seconds.

3.2 Instrument Deconvolution of the Data

The transfer function in the s-plane of the seismic recording instruments and seismometers was obtained in the first step of instrument deconvolution. An expression for each stage of the seismic recording instruments was calculated using Laplace transform theory and laboratory testing; the general s-plane expression for the seismometers is derived in the Appendix.

A computer program was written by Cumming which calculated the amplitude and phase spectra, as well as impulse response, for a given transfer function. The program used a basic Fourier transform subroutine, FASTFT, which made use of subroutines COSP, COSTAB, SINTAB, and SPLIT (Robinson, 1966). The amplitude and phase spectra were calculated over a frequency range from one-hundredth to one hundred Hertz; the impulse responses were sampled at an interval of 0.0056 seconds for 1.25 seconds; and all plots were done using a model 770/663 CALCOMP Plotter at the University of Alberta Computing Center.

The impulse response of the seismic recording instruments and seismometers used at the University of Alberta in 1971 was generated and truncated after forty-three samples; it was then input to a program

which used subroutine SPIKE, which made use of subroutines IMPULS, SHAPE, CROSS, EUREKA, DOT, FOLD, ZERO, and MINSN (Robinson, 1967). SPIKE was used to compute a spiking filter which could be convolved with the truncated impulse response to give an approximation to a delta function. The spiking filter was then convolved with the data to give data which had been instrument deconvolved.

Let $b_0,b_1,b_2,\ldots,b_n$ be the truncated impulse response, and let $d_0,d_1,d_2,\ldots,d_{m+n}$ be the desired output, a delta function, which has all its coefficients equal to zero except a single coefficient which is equal to one. The purpose of SPIKE is to find a spiking filter $f_0,f_1,f_2,\ldots,f_m$ such that when we convolve the truncated impulse response with the spiking filter, we obtain an output wavelet $c_0,c_1,c_2,\ldots,c_{m+n}$ which is as close as possible to the desired output in a least-squares sense.

The spiking filter is calculated so that the sum of squares given by

$$I = \sum_{t=0}^{m+n} (c_t - d_t)^2 \qquad 3.1$$

is a minimum. Substituting for c_t, we have

$$I = \sum_{t=0}^{m+n} \left(\sum_{s=0}^{m} f_s b_{t-s} - d_t \right)^2 . \qquad 3.2$$

The value of I is a minimum if its partial derivatives with respect to each of the coefficients $f_0, f_1, f_2, \ldots, f_m$ are equal to zero. Thus, we have

$$\frac{\partial I}{\partial f_j} = \sum_{t=0}^{m+n} 2\left(\sum_{s=0}^{m} f_s b_{t-s} - d_t \right)\left(b_{t-j} \right) = 0 \ , \qquad 3.3$$

which is, for $j = 0,1,2,\ldots,m$,

$$\sum_{s=0}^{m} f_s \left(\sum_{t=0}^{m+n} b_{t-s} b_{t-j} \right) = \sum_{t=0}^{m+n} d_t b_{t-j} \ . \qquad 3.4$$

The autocorrelation of the truncated impulse response is defined as, using equation 2.2,

$$r_{j-s} = \sum_{t=0}^{m+n} b_{t-s} b_{t-j}$$

where the $b_0, b_1, b_2, \ldots, b_n$ are real. Similarly, the cross correlation between the desired output and the truncated impulse response is defined as

$$g_j = \sum_{t=0}^{m+n} d_t b_{t-j} \ , \quad \text{for all} \quad j = 0,1,2,\ldots,m \ . \qquad 3.5$$

The set of equations in 3.4 reduces to

$$g_j = \sum_{s=0}^{m} f_s r_{j-s} \ , \quad \text{for all} \quad j = 0,1,2,\ldots,m \ . \qquad 3.6$$

This set of m+1 simultaneous linear equations in the unknown coefficients $f_0, f_1, f_2, \ldots, f_m$ is the discrete time analog of the Wiener-Hopf integral equation (Robinson, 1967). The equations are called the normal equations for the filter.

The spiking filter was arbitrarily chosen to be of length forty-three, since the least-squares error decreased monotonically as the length of the spiking filter increased. SPIKE was used to calculate the least-squares error for each of the possible positions of the one in the delta function; the error was a minimum when the one was in the twenty-ninth position.

The spiking filter was convolved with the data obtained at the University of Alberta in 1971. The original data, filtered by a five to thirty Hertz zero phase shift eight pole Butterworth bandpass filter (Alpaslan, 1968), is plotted in Figure 3.4. The data, convolved with the spiking filter and filtered with the same bandpass filter as before, is plotted in Figure 3.5. Although the two plots are very similar, there is a definite sharpening of several three sided pulses into two sided pulses. The resulting two sided pulses resemble the half cycle sine wave pulses obtained for the Pierre Shale (McDonal et al., 1958). The instrument deconvolution is thus moderately successful.

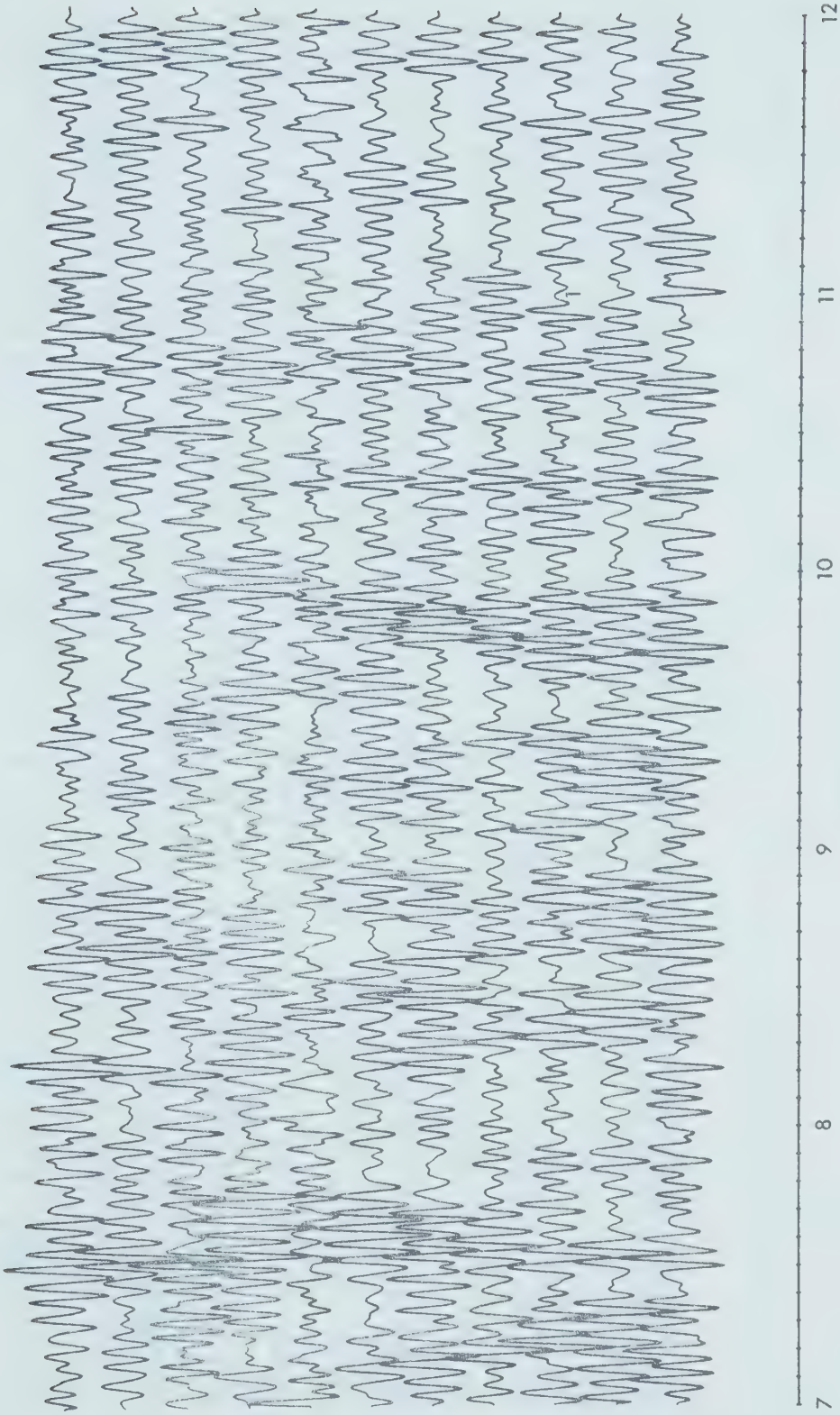

Figure 3.4. Eleven channels of data from the first shot on September 2, 1971 before instrument deconvolution.

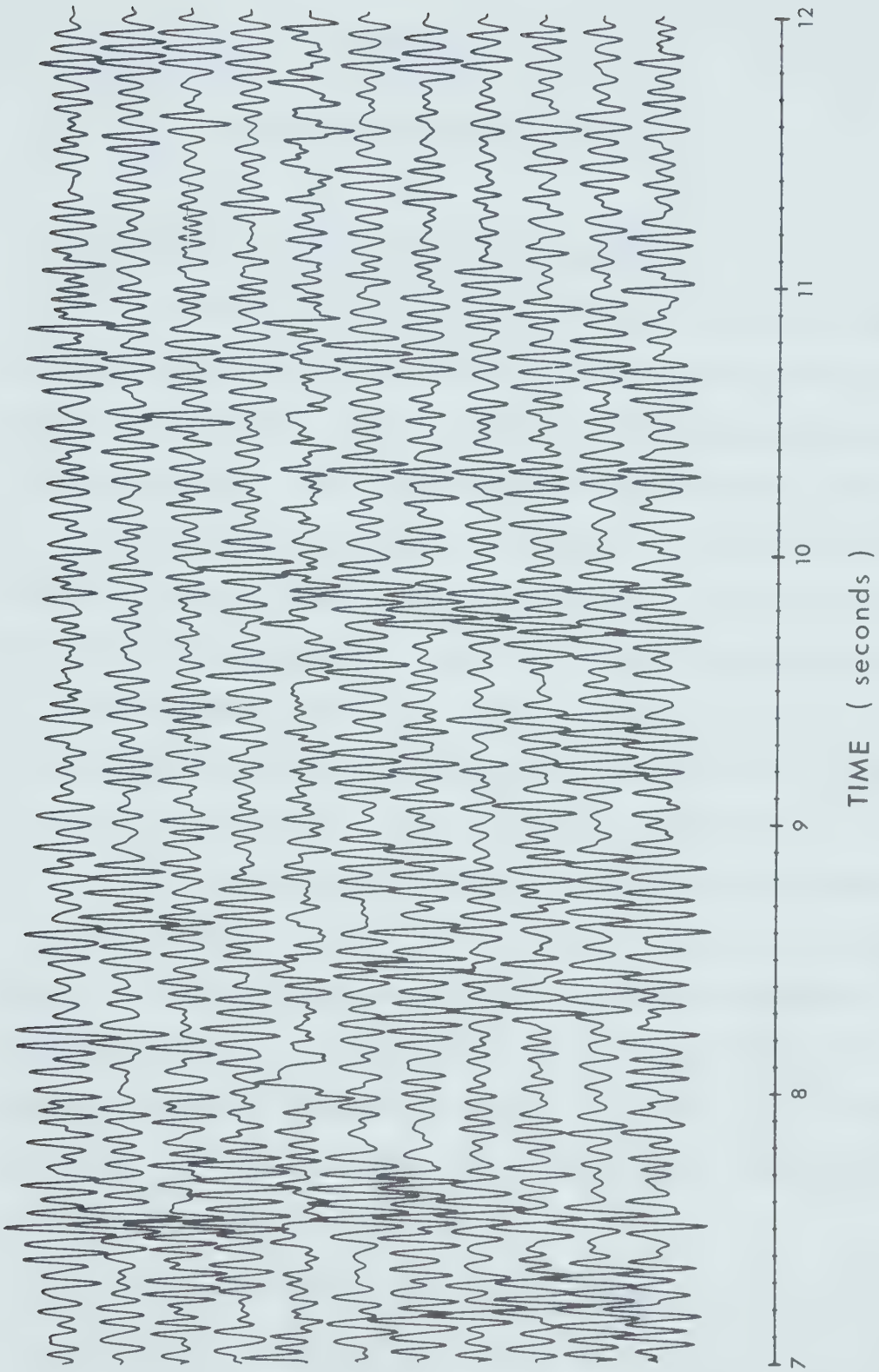

Figure 3.5. Eleven channels of data from the first shot on September 2, 1971 after instrument deconvolution.

CHAPTER 4

PREDICTIVE DECONVOLUTION

4.1 The Predictive Decomposition Theorem

The following discussion of the Predictive Decomposition Theorem and of the method of predictive deconvolution is based largely on three references (Robinson, 1954; Robinson, 1967; and Peacock and Treitel, 1969).

Any observational time series x_t $(-\infty < t < \infty)$ may be considered as a realization of a random process, which is a mathematical abstraction defined with respect to a probability field. A time series is said to be stationary if the probabilities involved in the random process do not have a specific origin in time.

For any random process, averages may be taken with respect to the ensemble of realizations x_t for a fixed time t; such averages are called ensemble averages. The ensemble average or mean value of x_t is denoted by $E[x_t]$, and the variance is denoted by $E[(x_t - E(x_t])^2]$; both the mean and the variance of a stationary random process are independent of time.

The autocorrelation coefficients

$$\phi_{xx}(t) = E[x_{s+t}x_s] \qquad 4.1$$

are independent of s, and they are an even function of

the time t, that is

$$\phi_{xx}(t) = \phi_{xx}(-t) \quad . \tag{4.2}$$

Another type of average is the time average, taken with respect to all values of time t for a fixed realization x_t $(-\infty < t < \infty)$ of the random process. A stationary process is called an ergodic process if the ensemble averages and the time averages are equal with probability one. As a result, the autocorrelation of an ergodic process may be expressed as a time average, as in earlier chapters.

The autocorrelation is a non-negative definite function; that is, equation 4.2 holds, and

$$\sum_{j=1}^{n} \sum_{k=1}^{n} \phi_{xx}(j-k) a_j a_k \geq 0 \quad , \quad n = 1,2,3,\ldots, \tag{4.3}$$

for every real set of $a_1, a_2, a_3, \ldots, a_n$ (Robinson, 1954). This property of the autocorrelation is equivalent to its representation by the Fourier transform

$$\phi_{xx}(t) = \frac{1}{\pi} \int_0^{\pi} \cos \omega t \, d\Lambda(\omega) \quad , \tag{4.4}$$

a representation known as the Wiener-Khintchine theorem. The spectral distribution function $\Lambda(\omega)$ is a real monotonically increasing function of ω $(0 \leq \omega \leq \pi)$ with $\Lambda(0) = 0$ and $\Lambda(\pi) = \pi$. The inversion formula is

$$\Lambda(\omega) = \omega + 2 \sum_{t=1}^{\infty} \frac{\phi_{xx}(t)}{t} \sin \omega t \ , \qquad 4.5$$

$0 \leq \omega \leq \pi$.

If $\sum_{t=0}^{\infty} |\phi_{xx}(t)|$ is convergent, then the spectral distribution function will be absolutely continuous, with the continuous derivative

$$\Phi(\omega) = \frac{d\Lambda(\omega)}{d\omega} \ , \qquad 4.6$$

where $\Phi(\omega)$ is the power spectrum, an even, non-negative function. In terms of the power spectrum, the auto-correlation is

$$\phi_{xx}(t) = \frac{1}{2\pi} \int_{-\pi}^{\pi} \exp(i\omega t)\ \Phi(\omega)\ d\omega \ . \qquad 4.7$$

A time series with an absolutely continuous spectral distribution function is generated by a process of convolution. For a fixed realization of white noise $\ldots,e_{t-1},e_t,e_{t+1},\ldots$, the corresponding fixed realization of a process of convolution is $\ldots,x_{t-1},x_t,x_{t+1},\ldots$ where

$$x_t = \sum_{s=-\infty}^{\infty} c_s e_{t-s} \quad \text{for all } t, \ -\infty < t < \infty \ . \qquad 4.8$$

It may be assumed that the e_t are mutually uncorrelated, and that the mean and the variance of the e_t are zero and one, respectively; then

$$E[e_s e_t] = E[e_s]\ E[e_t] = 0 \quad \text{for} \quad s \neq t \ . \qquad 4.9$$

The autocorrelation coefficients of a process of convolution x_t may be written

$$\phi_{xx}(t) = E[\sum_{j=-\infty}^{\infty} c_j e_{s+t-j} \sum_{k=-\infty}^{\infty} c_k e_{s-k}]$$

$$= E[\sum_{j=-\infty}^{\infty} \sum_{k=-\infty}^{\infty} c_j c_k e_{s+t-j} e_{s-k}]$$

$$= \sum_{j=-\infty}^{\infty} \sum_{k=-\infty}^{\infty} c_j c_k \, E[e_{s+t-j} e_{s-k}]$$

$$= \sum_{j=-\infty}^{\infty} c_j c_{j-t} \quad . \qquad 4.10$$

By using the relationship

$$\int_{-\pi}^{\pi} \exp(i\omega j)\exp(-i\omega k)\, d\omega = \begin{cases} 2\pi & j = k \\ 0 & j \neq k \end{cases} ,$$

the autocorrelation may be written

$$\phi_{xx}(t) = \frac{1}{2\pi} \int_{-\pi}^{\pi} \exp(i\omega t) \sum_{j=-\infty}^{\infty} c_j \exp(i\omega j) \sum_{k=-\infty}^{\infty} c_k \exp(-i\omega k)\, d\omega, \qquad 4.11$$

which is in the form of equation 4.7 where

$$\Phi(\omega) = |C(\omega)|^2 = \sum_{j=-\infty}^{\infty} c_j \exp(i\omega j) \sum_{k=-\infty}^{\infty} c_k \exp(-i\omega k), \qquad 4.12$$

$C(\omega)$ being the transfer function of the operator c_t. Thus, the spectral distribution function is absolutely

continuous. Conversely, any process with an absolutely continuous spectral distribution function is a process of convolution.

It may be shown that a process with a power spectrum $\Phi(\omega)$ may be made physically realizable, stable, and minimum-delay by using the Kolmogorov factorization of the spectrum or the Fejer factorization method (Robinson, 1954). That is, the power spectrum may be factored

$$\Phi(\omega) = |B(\omega)|^2 = \left| \sum_{t=0}^{\infty} b_t \exp(-i\omega t) \right|^2 , \qquad 4.13$$

where $b_t = 0$ for $t < 0$, $b_0 > 0$,

$$\sum_{t=0}^{\infty} b_t^2 < \infty , \quad \sum_{t=0}^{\infty} |b_t| < \infty, \quad \text{and}$$

$$\sum_{t=0}^{\infty} b_t z^t \neq 0 \quad \text{for} \quad |z| \leq 1 \quad . \qquad 4.14$$

It may be seen that equation 4.13 may be used in place of equation 4.12; in other words, the operator $c_0, c_1, c_2, \ldots$ may be replaced by the operator $b_0, b_1, b_2, \ldots$. Thus the process of convolution is given by

$$x_t = \sum_{s=0}^{\infty} b_s e_{t-s} \quad , \quad -\infty < t < \infty \quad , \qquad 4.15$$

replacing equation 4.8 with its minimum-delay equivalent. In this equation, the e_t $(-\infty < t < \infty)$ represent a realization of a mutually uncorrelated process with zero mean

and unit variance, that is, white noise.

The Predictive Decomposition Theorem may now be stated. Given a non-deterministic stationary process x_t $(-\infty < t < \infty)$ with discrete time parameter t, suppose x_t has an absolutely continuous spectral distribution function. Then there exists a decomposition

$$x_t = b_0 e_t + b_1 e_{t-1} + b_2 e_{t-2} + \ldots , \qquad 4.16$$

where the e_t have zero mean and unit variance and are mutually uncorrelated, and the operator $b_0, b_1, b_2, \ldots$ is minimum-delay with $b_0 > 0$ and $b_0^2 + b_1^2 + b_2^2 + \ldots < \infty$. This may be described as the minimum-delay specialization of the Wold Decomposition Theorem (Robinson, 1954).

Because the operator $b_0, b_1, b_2, \ldots$ is minimum-delay, there exists an inverse operator $a_0, a_1, a_2, \ldots$ which is realizable and minimum-delay. Thus we have the inverse predictive decomposition of the time series x_t given by

$$e_t = a_0 x_t + a_1 x_{t-1} + a_2 x_{t-2} + \ldots . \qquad 4.17$$

4.2 Single Channel Predictive Deconvolution

The model required for the application of predictive deconvolution is based on the hypothesis that the strengths and arrival times of the signals in a seismic trace can be represented as white noise, and on the

hypothesis that the characteristic wavelet associated with each signal is minimum-delay.

The prediction of $x_{t+\alpha}$ by $\hat{x}_{t+\alpha}$ is

$$\hat{x}_{t+\alpha} = \sum_{s=0}^{\infty} b_{\alpha+s} e_{t-s} = \sum_{s=0}^{\infty} b_{\alpha+s} \sum_{n=0}^{\infty} a_n x_{t-s-n} \qquad 4.18$$

using equations 4.16 and 4.17. Now let $r = s+n$; then

$$\hat{x}_{t+\alpha} = \sum_{s=0}^{\infty} b_{\alpha+s} \sum_{r=0}^{\infty} a_{r-s} x_{t-r} = \sum_{r=0}^{\infty} \left(\sum_{s=0}^{\infty} b_{\alpha+s} a_{r-s} \right) x_{t-r} . \qquad 4.19$$

Now, define the filter operator $f_0, f_1, f_2, \ldots$, where

$$f_r(\alpha) = \sum_{s=0}^{\infty} b_{\alpha+s} a_{r-s} \qquad 4.20$$

so that equation 4.19 becomes

$$\hat{x}_{t+\alpha} = \sum_{r=0}^{\infty} f_r(\alpha) x_{t-r} = f_0(\alpha) x_t + f_1(\alpha) x_{t-1} + f_2(\alpha) x_{t-2} + \ldots . \qquad 4.21$$

Thus, $\hat{x}_{t+\alpha}$ is expressed in terms of a linear combination of the present x_t and the past $x_{t-1}, x_{t-2}, x_{t-3}, \ldots$. The operator $f_0, f_1, f_2, \ldots$ is realizable since $f_r(\alpha)$ is zero for r less than zero (Robinson, 1954).

In practical applications, only a finite number of the past x_t may be used in the prediction of $x_{t+\alpha}$. Therefore, define

$$\hat{x}_{t+\alpha} = f_0 x_t + f_1 x_{t-1} + f_2 x_{t-2} + \ldots + f_m x_{t-m} \quad . \tag{4.22}$$

Using the method of least-squares, the value of

$$I = \sum_{t=-\infty}^{\infty} (x_{t+\alpha} - \hat{x}_{t+\alpha})^2 \tag{4.23}$$

must be minimized. Substitution for $\hat{x}_{t+\alpha}$ gives

$$I = \sum_{t=-\infty}^{\infty} \left(x_{t+\alpha} - (f_0 x_t + f_1 x_{t-1} + f_2 x_{t-2} + \ldots + f_m x_{t-m}) \right)^2 \quad . \tag{4.24}$$

The value of I is a minimum if its partial derivatives with respect to each of the $f_0, f_1, f_2, \ldots, f_m$ are equal to zero. Then

$$\frac{\partial I}{\partial f_j} = \sum_{t=-\infty}^{\infty} 2 \left(x_{t+\alpha} - (f_0 x_t + f_1 x_{t-1} + f_2 x_{t-2} + \ldots + f_m x_{t-m}) \right) \times \times (-x_{t-j}) = 0 \quad , \tag{4.25}$$

which is, substituting the autocorrelation of X from equation 2.2,

$$f_0 r_j + f_1 r_{j-1} + f_2 r_{j-2} + \ldots + f_m r_{j-m} = r_{\alpha+j} \quad ,$$

$$\text{for } j = 0,1,2,\ldots,m \quad . \tag{4.26}$$

Therefore, the filter operator $f_0, f_1, f_2, \ldots, f_m$ is given as the solution of these normal equations. The solution

is found by a recursive algorithm; if the filter operator is of length m, machine time is proportional to m^2, while computer storage is proportional to m (Robinson, 1967).

In matrix form, equation 4.26 is

$$\begin{pmatrix} r_0 & r_1 & r_2 & \cdots & r_m \\ r_1 & r_0 & r_1 & & r_{m-1} \\ r_2 & r_1 & r_0 & & r_{m-2} \\ \vdots & & & & \vdots \\ r_m & r_{m-1} & r_{m-2} & \cdots & r_0 \end{pmatrix} \begin{pmatrix} f_0 \\ f_1 \\ f_2 \\ \vdots \\ f_m \end{pmatrix} = \begin{pmatrix} r_\alpha \\ r_{\alpha+1} \\ r_{\alpha+2} \\ \vdots \\ r_{\alpha+m} \end{pmatrix} . \qquad 4.27$$

The autocorrelation matrix on the left is symmetric, has its elements equal along each diagonal, has non-negative eigenvalues, and has a non-negative determinant.

The prediction error time series is defined as

$$\hat{e}_{t+\alpha} = x_{t+\alpha} - \hat{x}_{t+\alpha} = x_{t+\alpha} - f_0 x_t - f_1 x_{t-1} - f_2 x_{t-2} - \cdots - f_m x_{t-m}$$

$$= a_0 x_{t+\alpha} + a_1 x_{t+\alpha-1} + a_2 x_{t+\alpha-2} + \cdots + a_{\alpha+m} x_{t-m} \qquad 4.28$$

where

$$(a_0, a_1, a_2, \ldots, a_{\alpha+m}) = (1, 0, 0, 0, \ldots, 0, -f_0, -f_1, -f_2, \ldots, -f_m) . \qquad 4.29$$

From equation 4.24, the least-squares error is

$$I_0 = \sum_{t=-\infty}^{\infty} \left((x_{t+\alpha} - \sum_{j=0}^{m} f_j x_{t-j})^2 \right)$$

$$= \sum_{t=-\infty}^{\infty} \left(x_{t+\alpha}^2 - 2 \sum_{j=0}^{m} f_j x_{t+\alpha} x_{t-j} + \sum_{j=0}^{m} f_j \sum_{k=0}^{m} f_k x_{t-j} x_{t-k} \right)$$

$$= r_0 - 2 \sum_{j=0}^{m} f_j r_{\alpha+j} + \sum_{j=0}^{m} f_j \left(\sum_{k=0}^{m} f_k r_{j-k} \right) \quad . \qquad 4.30$$

Using equation 4.26 to evaluate the term in brackets, the least-squares error is

$$I_0 = r_0 - \sum_{j=0}^{m} f_j r_{\alpha+j} = \sum_{j=0}^{m+\alpha} a_j r_j \quad . \qquad 4.31$$

Equation 4.27, in matrix form, may be rewritten as a system of m+1 simultaneous linear equations,

$$\begin{aligned}
r_0 f_0 + r_1 f_1 + r_2 f_2 + \ldots + r_m f_m &= r_\alpha \\
r_1 f_0 + r_0 f_1 + r_1 f_2 + \ldots + r_{m-1} f_m &= r_{\alpha+1} \\
r_2 f_0 + r_1 f_1 + r_0 f_2 + \ldots + r_{m-2} f_m &= r_{\alpha+2} \\
&\vdots \\
r_m f_0 + r_{m-1} f_1 + r_{m-2} f_2 + \ldots + r_0 f_m &= r_{\alpha+m} \quad .
\end{aligned} \qquad 4.32$$

This system of equations may be augmented in such a way that the prediction operator is converted to its corresponding prediction error operator (Peacock and Treitel, 1969). The matrix equation corresponding to the augmented

system of equations is

$$\begin{pmatrix} r_0 & r_1 & r_2 & \cdots & r_{\alpha+m} \\ r_1 & r_0 & r_1 & & r_{\alpha+m-1} \\ r_2 & r_1 & r_0 & & r_{\alpha+m-2} \\ \vdots & & & & \vdots \\ r_{\alpha-1} & r_{\alpha-2} & r_{\alpha-3} & & r_{m+1} \\ r_\alpha & r_{\alpha-1} & r_{\alpha-2} & & r_m \\ \vdots & & & & \vdots \\ r_{\alpha+m} & r_{\alpha+m-1} & r_{\alpha+m-2} & \cdots & r_0 \end{pmatrix} \begin{pmatrix} 1 \\ 0 \\ 0 \\ \vdots \\ 0 \\ -f_0 \\ \vdots \\ -f_m \end{pmatrix} = \begin{pmatrix} \beta_0 \\ \beta_1 \\ \beta_2 \\ \vdots \\ \beta_{\alpha-1} \\ 0 \\ \vdots \\ 0 \end{pmatrix}, \qquad 4.33$$

where

$$\beta_j = r_j - (r_{\alpha-j} f_0 + r_{\alpha-j+1} f_1 + r_{\alpha-j+2} f_2 + \ldots + r_{\alpha-j+m} f_m) . \qquad 4.34$$

Thus, the prediction operator of equation 4.27 has been converted to its corresponding prediction error operator.

For the case $\alpha = 1$, equation 4.33 becomes

$$\begin{pmatrix} r_0 & r_1 & r_2 & \cdots & r_{m+1} \\ r_1 & r_0 & r_1 & & r_m \\ r_2 & r_1 & r_0 & & r_{m-1} \\ \vdots & & & & \vdots \\ r_{m+1} & r_m & r_{m-1} & \cdots & r_0 \end{pmatrix} \begin{pmatrix} 1 \\ -f_0 \\ -f_1 \\ \vdots \\ -f_m \end{pmatrix} = \begin{pmatrix} \beta_0 \\ 0 \\ 0 \\ \vdots \\ 0 \end{pmatrix}, \qquad 4.35$$

where

$$\beta_0 = r_0 - (r_1 f_0 + r_2 f_1 + r_3 f_2 + \ldots + r_{m+1} f_m) \quad . \qquad 4.36$$

Equation 3.6 may be written in matrix form, setting $g_0 = 1$, $g_1 = 0$, $g_2 = 0$, $g_3 = 0$, ..., $g_{m+1} = 0$, recalling that the autocorrelation is an even function, and changing m to m+1,

$$\begin{bmatrix} r_0 & r_1 & r_2 & \cdots & r_{m+1} \\ r_1 & r_0 & r_1 & & r_m \\ r_2 & r_1 & r_0 & & r_{m-1} \\ \vdots & & & & \vdots \\ r_{m+1} & r_m & r_{m-1} & \cdots & r_0 \end{bmatrix} \begin{bmatrix} f_0 \\ f_1 \\ f_2 \\ \vdots \\ f_{m+1} \end{bmatrix} = \begin{bmatrix} 1 \\ 0 \\ 0 \\ \vdots \\ 0 \end{bmatrix} \quad . \qquad 4.37$$

But this equation is the one for the calculation of the least-squares inverse filter which compresses an unknown signal into a unit spike at zero delay (Peacock and Treitel, 1969). Comparing equation 4.37 to equation 4.35, it may be seen that the m+2 length prediction error operator with unit prediction distance is identical to the zero delay, least-squares inverse filter of length m+2, except for a scale factor β_0.

Similarly, equation 4.33 may be compared to equation 3.6; then $g_0 = \beta_0$, $g_1 = \beta_1$, $g_2 = \beta_2$, ..., $g_{\alpha-1} = \beta_{\alpha-1}$, $g_\alpha = 0$, ..., $g_{\alpha+m} = 0$. The solution of equation 3.6, changing m to α+m, is a least-squares inverse filter of length α+m+1; the solution of equation

4.33 is the prediction error operator of length $\alpha+m+1$ for the prediction distance of α; therefore, these two filters are identical.

Using equation 4.10, the autocorrelation of the input may be considered to be the autocorrelation of the characteristic wavelet. But limiting the positive lag half of the autocorrelation to length $\alpha+m+1$ implies that the characteristic wavelet is of length $\alpha+m+1$.

Since $g_j = 0$ for $\alpha \leq j \leq \alpha+m$, and since g_j is the cross-correlation between the desired output and the input, the cross-correlation is zero for lags greater than $\alpha-1$. Therefore, it may be concluded that the desired output is of length α. Since the desired output is of length α, its autocorrelation is zero at lags α, $\alpha+1$, $\alpha+2$, ... The prediction error filter will modify the input in such a way that the autocorrelation of the output will tend to be zero at lags α, $\alpha+1$, $\alpha+2$, ... , $\alpha+m$.

The prediction error operator contracts the characteristic wavelet of length $\alpha+m+1$ into a wavelet of length α. Least-squares inverse filtering contracts a characteristic wavelet of length $\alpha+m+1$ into a wavelet of length 1. Thus, it may be concluded that predictive deconvolution is a generalized method of least-squares inverse filtering in which the degree of wavelet contraction may be controlled.

4.3 Test of Reverberation Removal

Removal of predictable energy from data is possible if the method of predictive deconvolution is used; the energy removed will have periods between α and $\alpha+m$ time intervals, and it may be classed as either short period or long period energy. The first step is to plot the positive lag half of the autocorrelation. Short period reverberations will appear as decaying waveforms on the autocorrelation plot, while long period reverberations will appear as distinct waveforms separated by quiet intervals.

Removing short period reverberations is done differently depending on whether or not the decaying waveform on the autocorrelation plot is highly regular. If the waveform is highly regular, α is set at the desired prediction distance while $\alpha+m+1$ is set to span α plus one complete cycle. If the waveform is irregular, α is set at the desired prediction distance while $\alpha+m+1$ is set to span α plus the remaining significant interval. In either case, α should be set to span the interval between zero lag and the second zero crossing on the autocorrelation plot (Peacock and Treitel, 1969).

Removing long period reverberations is done differently depending on whether or not the ringing is of a first order nature. If the ringing is of a first order nature, α is set to span the interval

between zero lag and the onset of the first multiple on the autocorrelation plot, while $\alpha+m+1$ spans α plus the first multiple. If the ringing is of a higher order nature, α is again set to span the interval between zero lag and the onset of the first multiple on the autocorrelation plot, while $\alpha+m+1$ spans α plus the first two or more multiples. In either case, repetitions of the waveform centered at multiples of $\alpha + (m+1)/2$ will be removed (Peacock and Treitel, 1969).

In order to test the effectiveness of the method of predictive deconvolution, a trial trace was created. This trace used the trial wavelet of Chapter Two; the trial wavelet was convolved with the trace $e_0 = 1$, $e_1 = 0$, $e_2 = 0$, ..., $e_{29} = 0$, $e_{30} = -1$; the trial trace is plotted on the upper left of Figures 4.1, 4.2, and 4.3. The autocorrelation plot of the trial trace is plotted on the upper right of Figures 4.1 and 4.3.

A main program was written to do single channel predictive deconvolution, using subroutine EUREKA (Robinson, 1967) to solve the normal equations (Robinson, 1964). An error in EUREKA's algorithm was found (Montalbetti, personal communication); an updated version of EUREKA was used by the main program.

In the study of short period reverberation removal, the trial trace was considered as a section of a time series composed of white noise, e_0, e_1, e_2, ..., e_{30},

Figure 4.1. Short period reverberation removal.
Upper left: the trial trace. Upper right: the autocorrelation plot of the trial trace.
Middle left: deconvolved trial trace - α=1, m=13.
Middle right: deconvolved trial trace - α=3, m=11.
Lower left: deconvolved trial trace - α=4, m=10.
Lower right: deconvolved trial trace - α=5, m=9.

Figure 4.2. Short period reverberation removal.
Upper left: the trial trace. Upper right: the autocorrelation plot of the deconvolved trial trace - $\alpha=4$, m=10.
Middle left: deconvolved trial trace - $\alpha=4$, m=9.
Middle right: deconvolved trial trace - $\alpha=4$, m=11.
Lower left: deconvolved trial trace - $\alpha=3$, m=10.
Lower right: deconvolved trial trace - $\alpha=5$, m=10.

Figure 4.3. Long period reverberation removal.
Upper left: the trial trace. Upper right: the autocorrelation plot of the trial trace.
Middle left: deconvolved trial trace - α=16, m=28.
Middle right: the autocorrelation plot of the deconvolved trial trace - α=16, m=28.
Lower left: deconvolved trial trace - α=16, m=27.
Lower right: deconvolved trial trace - α=4, m=40.

convolved with a characteristic wavelet, the trial wavelet. Since the time series is the convolution of a minimum-delay wavelet with white noise, equation 4.10 shows that the autocorrelation of the time series is the autocorrelation of the characteristic wavelet. When the autocorrelation of the trial trace was taken, the multiple on the autocorrelation plot was disregarded. To avoid errors due to the multiple, the section of the autocorrelation plot used was restricted to lags 0 to 15.

The two variables were α and m; in the following discussion, they will be written as a pair α-m; for example 4-10 would correspond to $\alpha = 4$ and $m = 10$. According to the criteria stated previously, the optimum case should be 6-8; that is, $\alpha = 6$, $m = 8$, and $\alpha+m+1 = 15$; $\alpha = 6$ is the lag corresponding to the second zero crossing on the autocorrelation plot, while $\alpha+m+1 = 15$ corresponds to the length of the characteristic wavelet and to the significant portion on the autocorrelation plot. The trials were taken by varying one of α or m while holding the other constant; other trials held $\alpha+m+1$ constant or else held $\alpha = 1$ constant, the case corresponding to zero delay least-squares inverse filtering. The best combination was 4-10; $\alpha = 4$ corresponds to the first negative maximum on the autocorrelation plot; the width of the

output spike is also 4. This case is plotted on the lower left of Figure 4.1, and its autocorrelation is plotted on the upper right of Figure 4.2. This autocorrelation plot shows the degree to which the autocorrelation approaches zero from lags α to $\alpha+m$ or lags 4 to 14.

When $\alpha+m+1$ was held constant at 15, increasing α caused the spike to become two sided and also added noise; the case 5-9 is plotted on the lower right of Figure 4.1. The supposedly optimum case 6-8 showed the spike as a two sided pulse with the second leg of greater amplitude than the first, and considerable noise was also evident. Decreasing α added noise; the cases 1-13 and 3-11 are plotted on the middle left and middle right of Figure 4.1, respectively.

When α was held constant at 4, little change was noted when m was increased or decreased; the cases 4-9 and 4-11 are plotted on the middle left and middle right of Figure 4.2, respectively.

When m was held constant at 10, increasing α caused the spike to become two sided and also added noise; decreasing α added noise. The cases 3-10 and 5-10 are plotted on the lower left and lower right of Figure 4.2, respectively.

When α was held constant at 1, the best output was at $\alpha+m+1 = 15$; the cases for m increasing or decreasing showed noise buildup, until noise was of the same amplitude as the signal. The case 1-13 is plotted on the middle left of Figure 4.1; these cases correspond to zero delay least-squares inverse filtering.

In the study of long period reverberation removal, the trial trace was considered as a section of a time series containing a reflection and a multiple of the same amplitude and shape but opposite sign. In this case, the multiple on the autocorrelation plot was regarded as real but undesirable.

The two variables α and m were unrestricted. According to the criteria stated previously, the optimum case should be 16-28; that is, $\alpha = 16$, $m = 28$, and $\alpha+m+1 = 45$; $\alpha = 16$ is the lag at which the first point of the multiple is seen on the autocorrelation plot, while $\alpha+m = 44$ is the lag at which the last point of the multiple is seen on the autocorrelation, and $\alpha+m+1 = 45$ is the length of the trial trace. The trials were taken by varying one of α or m while holding the other constant; other trials held $\alpha+m+1$ constant. The best combination was 16-28; this case is plotted on the middle left of Figure 4.3, and its autocorrelation is

plotted on the middle right of Figure 4.3. This autocorrelation plot shows the degree to which the autocorrelation approaches zero from lags α to $\alpha+m$ or lags 16 to 44. This case shows that the multiple has been reduced in amplitude by about one-half, but it also shows that a second multiple has been added.

When $\alpha+m+1$ was held constant at 45, increasing or decreasing α added low levels of noise which increased as α was further increased or decreased. The exception was the case 17-27 which is plotted on the lower left of Figure 4.3 and which shows a considerably higher level of noise.

When α was held constant at 15 or 16, little change was noticed as m was increased or decreased except the case 16-27 which shows a considerably higher level of noise.

When m was held constant at 27, 28, 39, or 30, little change was noted; however, when m was 27, a considerably higher level of noise was present.

One trial was done for the case 4-40; this case is plotted on the lower right of Figure 4.3; $\alpha = 4$ is the same as in the optimum short period case. This trial showed that short period and long period reverberations could be removed simultaneously.

4.4 Single Channel Predictive Deconvolution of Seismic Data

The method of single channel predictive deconvolution was tested on some of the seismic reflection data obtained at the University of Alberta in 1971. The data was chosen from the same shot on September 2, 1971 as was used in Chapter Three for instrument deconvolution; five channels were filtered by a five to thirty Hertz zero phase shift eight pole Butterworth bandpass filter; the time interval chosen was eighty-five samples long, from 7.25 to 7.73 seconds; the data is plotted on the left-hand side of Figures 4.4 and 4.5.

The single channel predictive deconvolution main program using subroutine EUREKA was used; the program operates on one channel at a time although its arrays are in multichannel form. The positive lag half of the autocorrelation is plotted in the center of Figures 4.4 and 4.5; a good degree of similarity between the autocorrelation plots may be seen. The first negative maximum on each autocorrelation plot occurs at lag 5, while the second zero crossing occurs between lags 7 and 8.

Since the short period reverberation removal tests indicated that the prediction distance α was the important parameter to determine, whereas the parameter

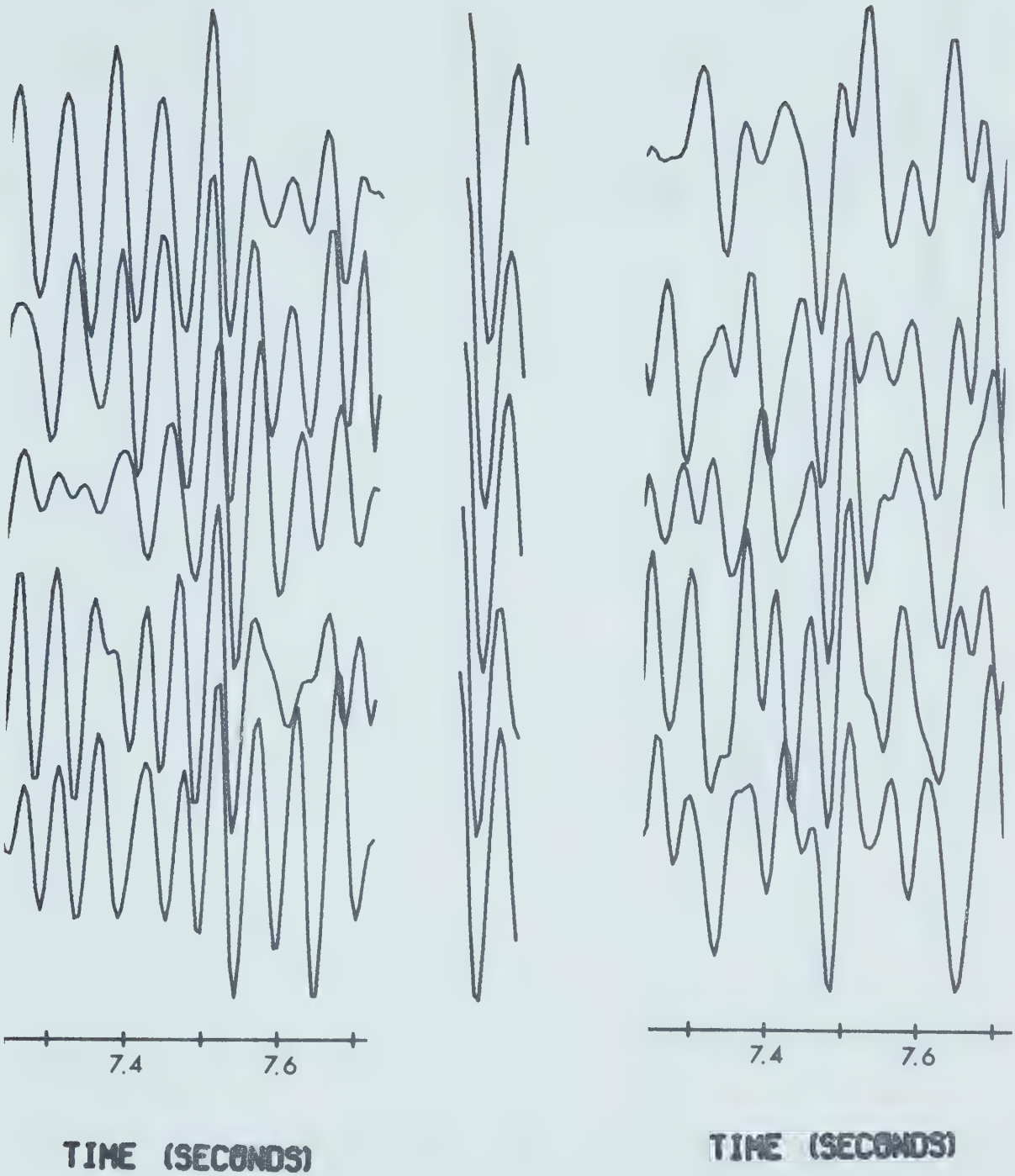

Figure 4.4. Single channel predictive deconvolution. Left-hand side: five channels of data from the first shot on September 2, 1971. Center: autocorrelation plots for the five channels of data. Right-hand side: five channels of deconvolved data with prediction distance $\alpha = 5$ and $\alpha+m+1 = 14$.

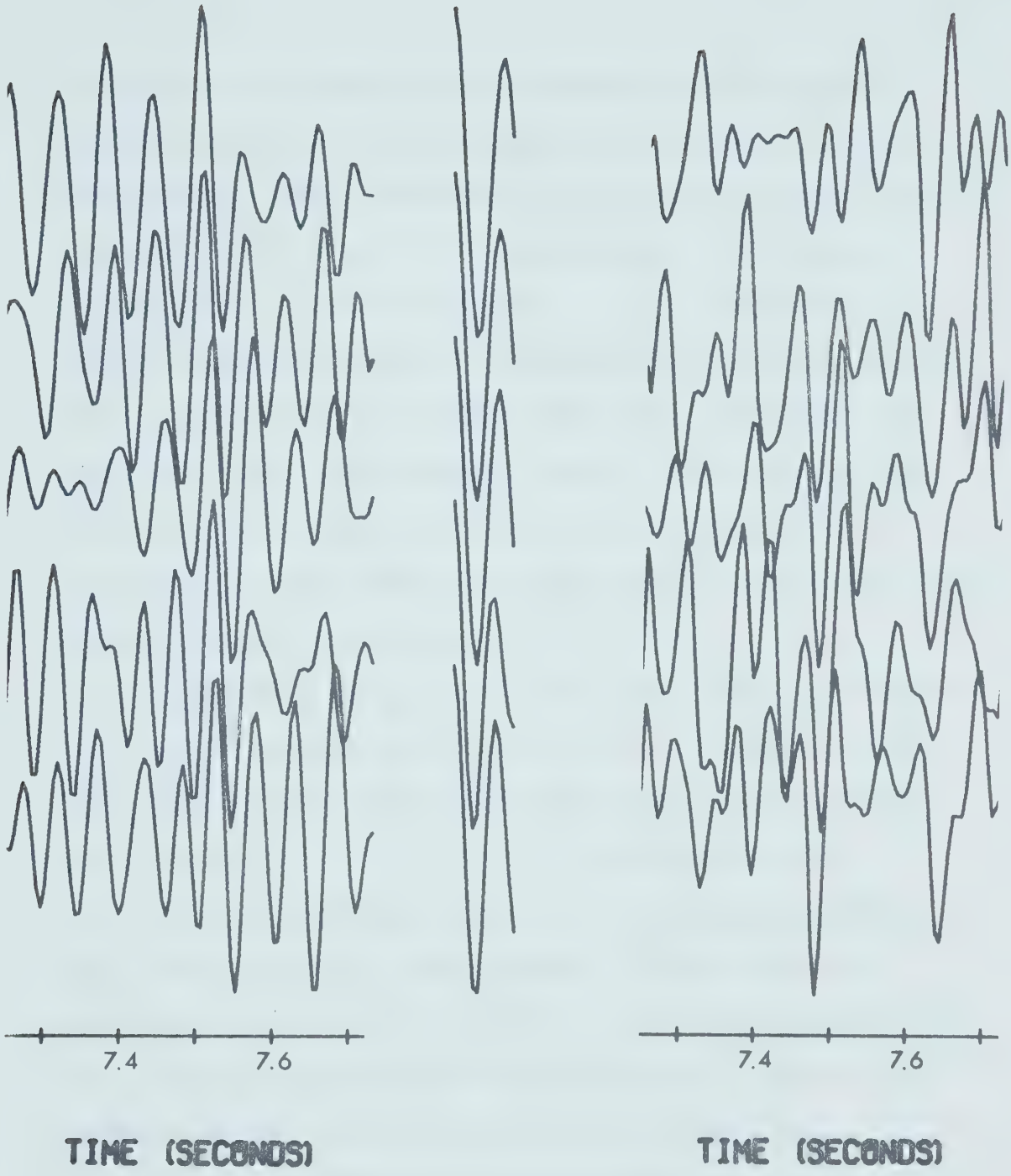

Figure 4.5. Single channel predictive deconvolution. Left-hand side: five channels of data from the first shot on September 2, 1971. Center: autocorrelation plots for the five channels of data. Right-hand side: five channels of deconvolved data with prediction distance $\alpha = 1$ and $\alpha+m+1 = 14$.

m had little effect and the parameter $\alpha+m+1$ was of only slightly more importance, a set of tests was run holding $\alpha+m+1$ constant at 18 while varying α from 1 to 12. With $\alpha+m+1 = 18$, two cycles of the auto-correlation plot were spanned. It was found that the changes between tests as α increased were very subtle; when α was 1 to 5, the main event was reduced to one leg, and when α was greater than 5, two or more legs seemed to be present. Thus, α was chosen to be 5, although it might have been chosen to be 4, 6, or 7 with little significant change.

The next set of tests was run holding α constant at 5 while setting $\alpha+m+1$ equal to 9, 11, 14, 17, and 20. Little difference was seen between the cases for $\alpha+m+1$ equal to 11, 14, or 17. According to the previously stated criterion, if the autocorrelations are highly regular, $\alpha+m+1$ is set to span α plus one complete cycle. One cycle on the autocorrelation plot was 9 lags, so $\alpha+m+1$ was chosen to be 14. This case is plotted on the right-hand side of Figure 4.4.

A final test was run with α set at 1 and $\alpha+m+1$ set at 14. This case corresponds to zero delay least-squares inverse filtering and is plotted on the right-hand side of Figure 4.5. It may be seen that the deconvolved data is somewhat sharper for this case than

for the case with α set at 5 and $\alpha+m+1$ set at 14. In both cases, the output data was filtered by a five to thirty Hertz zero phase shift eight pole Butterworth bandpass filter.

4.5 Multichannel Predictive Deconvolution

Multichannel seismic reflection data may be deconvolved by means of a multichannel least-squares inverse filter which is determined by requiring that the sum of the squared errors between the desired outputs and the actual outputs for each channel be minimized. This requirement leads to a set of simultaneous linear equations, called the normal equations, each element of which is itself a square matrix (Wiggins and Robinson, 1965).

Let the multichannel input be represented by x_t where t is an integer; then,

$$x_t = (x_{1t}, x_{2t}, x_{3t}, \ldots, x_{kt})^T , \qquad 4.38$$

where T denotes the matrix transpose. The filter is $f_0, f_1, f_2, \ldots, f_m$ where each f_j, $j = 0,1,2,\ldots,m$, is an $\ell \times k$ matrix. The actual multichannel output is

$$y_t = (y_{1t}, y_{2t}, y_{3t}, \ldots, y_{\ell t})^T . \qquad 4.39$$

The relationship between the input and the actual output

is given by

$$y_t = f_0 x_t + f_1 x_{t-1} + f_2 x_{t-2} + \ldots + f_m x_{t-m} \quad . \qquad 4.40$$

The desired multichannel output is

$$z_t = (z_{1t}, z_{2t}, z_{3t}, \ldots, z_{\ell t})^T \quad . \qquad 4.41$$

Therefore, it is required that

$$I = \sum_{i=1}^{\ell} E[(y_{it} - z_{it})^2] \qquad 4.42$$

be a minimum. When the multichannel input represents a multivariate random stationary process, the normal equations may be stated in matrix form as

$$\begin{pmatrix} r_0 & r_1 & r_2 & \cdots & r_m \\ r_1 & r_0 & r_1 & & r_{m-1} \\ r_2 & r_1 & r_0 & & r_{m-2} \\ \vdots & & & & \vdots \\ r_m & r_{m-1} & r_{m-2} & \cdots & r_0 \end{pmatrix} \begin{pmatrix} f_0 \\ f_1 \\ f_2 \\ \vdots \\ f_m \end{pmatrix} = \begin{pmatrix} g_0 \\ g_1 \\ g_2 \\ \vdots \\ g_m \end{pmatrix} , \qquad 4.43$$

where each r_j, $j = 0,1,2,\ldots,m$, is an autocorrelation coefficient of the input signal and is a $k \times k$ matrix, and where each g_j, $j = 0,1,2,\ldots,m$, is a cross-correlation coefficient between the desired output and the input and is an $\ell \times k$ matrix. That is,

$$r_t = E[x_{s+t}\, x_s^T] \quad , \qquad t = 0,1,2,\ldots,m \quad , \qquad 4.44$$

and

$$g_t = E[z_{s+t}\, x_s^T] \quad , \qquad t = 0,1,2,\ldots,m \quad . \qquad 4.45$$

In order to use equation 4.43 to do multichannel predictive deconvolution, the number of input channels must equal the number of output channels, that is, $k = \ell$. Then, the set of cross-correlation coefficients may be specified as

$$g_j = r_{\alpha+j} \quad , \qquad j = 0,1,2,\ldots,m \quad , \qquad 4.46$$

where α is the prediction distance. The set of filter coefficients $f_0, f_1, f_2, \ldots, f_m$ thus represents the multichannel prediction operator. The multichannel prediction error is defined to be

$$\hat{e}_{t+\alpha} = (x_{1t+\alpha}-y_{1t}, x_{2t+\alpha}-y_{2t}, x_{3t+\alpha}-y_{3t}, \ldots, x_{kt+\alpha}-y_{kt})^T \quad . \qquad 4.47$$

4.6 Multichannel Predictive Deconvolution of Seismic Data

The method of multichannel predictive deconvolution was tested on some of the seismic reflection data obtained at the University of Alberta in 1971. The data was chosen from the same shot on September 2, 1971 as was used in Chapter Three for instrument deconvolution;

however, the four channels chosen are not the same as the five channels used to test the method of single channel predictive deconvolution. The data was filtered by a five to thirty Hertz zero phase shift eight pole Butterworth bandpass filter; the time interval chosen was from 7.1 to 8.8 seconds; the data is plotted in Figure 4.6. The four channels were aligned by picking the initial trough on the event at 7.5 seconds; the shift from trace to trace was three samples.

A main program was written which used subroutine AUGURY, which made use of subroutines OMEN, FORM, MAINE, MOVE, ZERO, BRAINY, and HEAT (Robinson, 1967). AUGURY does multichannel predictive deconvolution for a prediction distance α equal to 1; MAINE calculates the inverse of a matrix; BRAINY does multichannel convolution; and HEAT calculates multichannel auto-correlations and cross-correlations.

With the alignment as specified, the data was deconvolved by multichannel prediction; it was found that three of the output traces were picked with peaks aligned but that the second trace from the top had troughs where the others had peaks, and vice-versa. One-half cycle of the dominant energy in the data was four samples; when the second trace was shifted by a positive or a negative lag of four samples, the traces

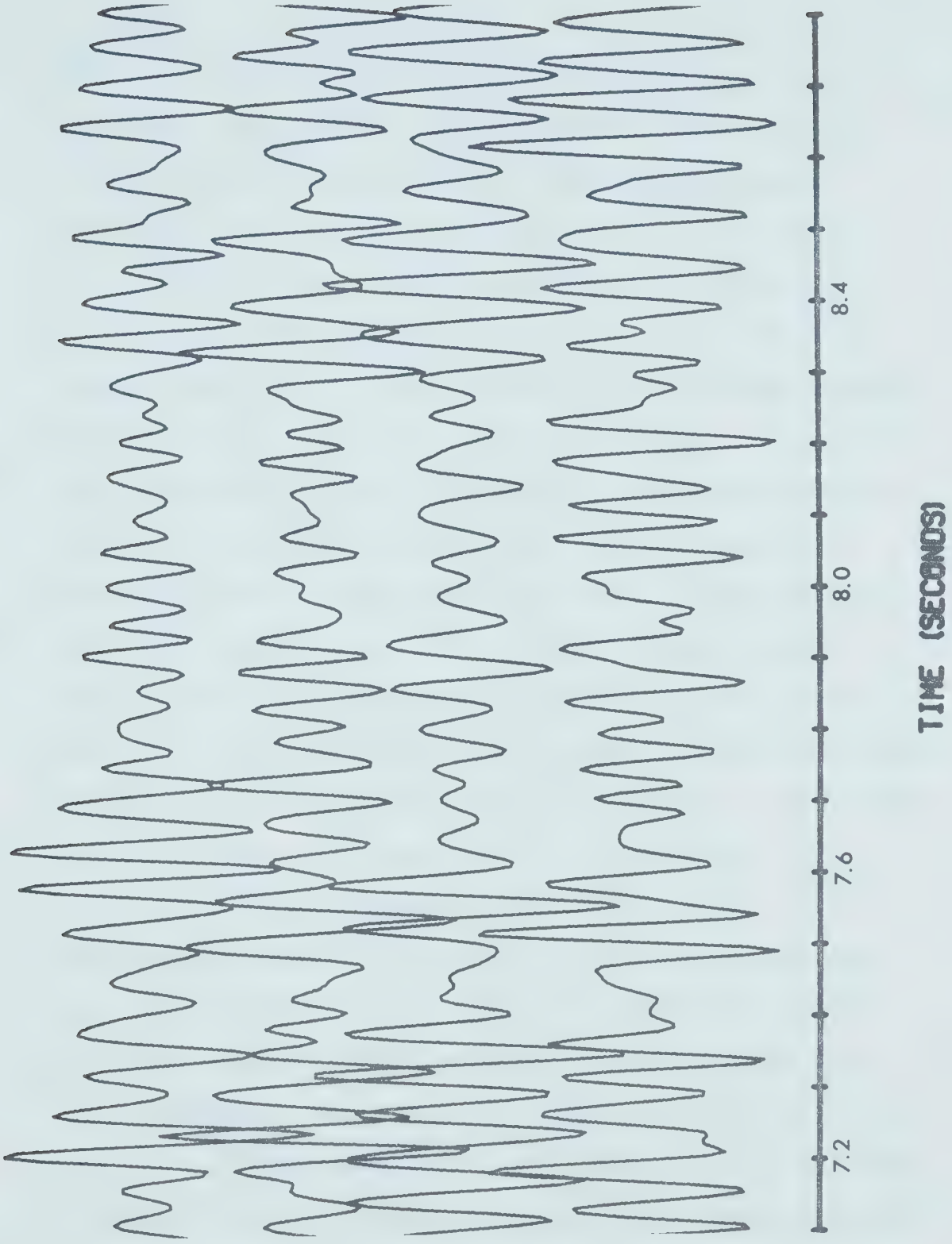

Figure 4.6. Four channels of data from the first shot on September 2, 1971. Each channel was filtered by a five to thirty Hertz Butterworth bandpass filter.

were all picked with positive peaks. The case for which the second trace was shifted by a negative lag of four samples was chosen for the remaining tests, and it is this case which is plotted in Figure 4.6.

A set of tests was run holding α constant at 1 and setting $\alpha+m+1$ equal to 3, 4, 5, ..., 10; thus, m ranged from 1 to 8. The case $\alpha+m+1 = 3$ was very similar to the original data; the similarity between output and input decreased as $\alpha+m+1$ increased. The cases $\alpha+m+1 = 9$ and 10 showed strong similarities between traces but few strong events and little similarity to the original data. The cases $\alpha+m+1 = 6$, 7, and 8 seemed to be a compromise; they showed some similarity to the original data, good similarities between traces, and strong events running across the traces. The case $\alpha+m+1 = 7$ was judged to be the best; this case is plotted in Figure 4.7.

As a comparison of the methods of single channel and of multichannel predictive deconvolution, the same four channels plotted in Figure 4.6 were deconvolved using the single channel main program which used subroutine EUREKA. The prediction distance α was set equal to 1 and $\alpha+m+1$ was set equal to 7; the output is plotted in Figure 4.8. The output from each method was filtered by a five to thirty Hertz zero phase shift eight pole Butterworth bandpass filter. It may be seen that the multichannel output in Figure 4.7 has slightly stronger

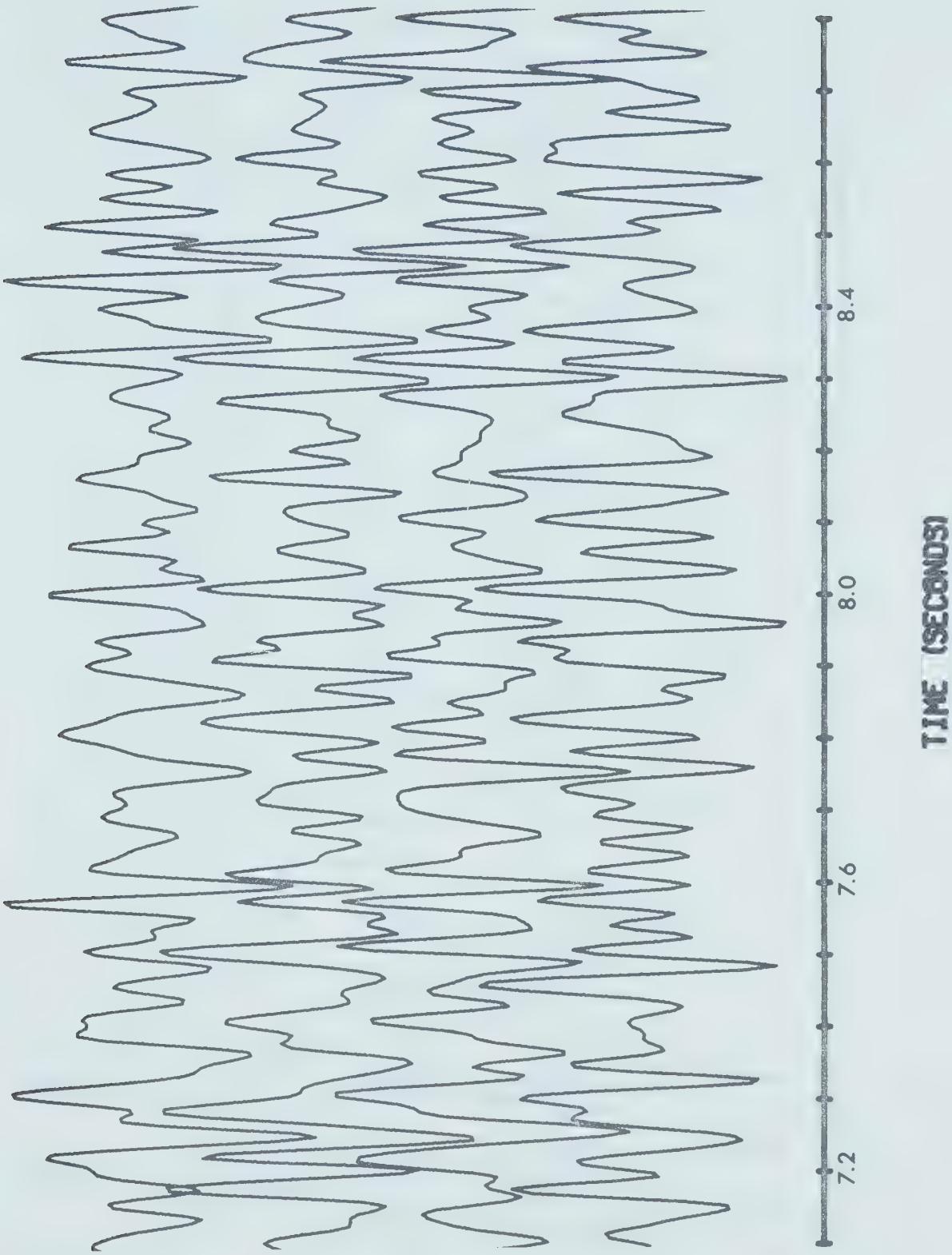

Figure 4.7. Multichannel predictive deconvolution. Four channels of data deconvolved by multichannel prediction with prediction distance $\alpha = 1$ and $\alpha+m+1 = 7$.

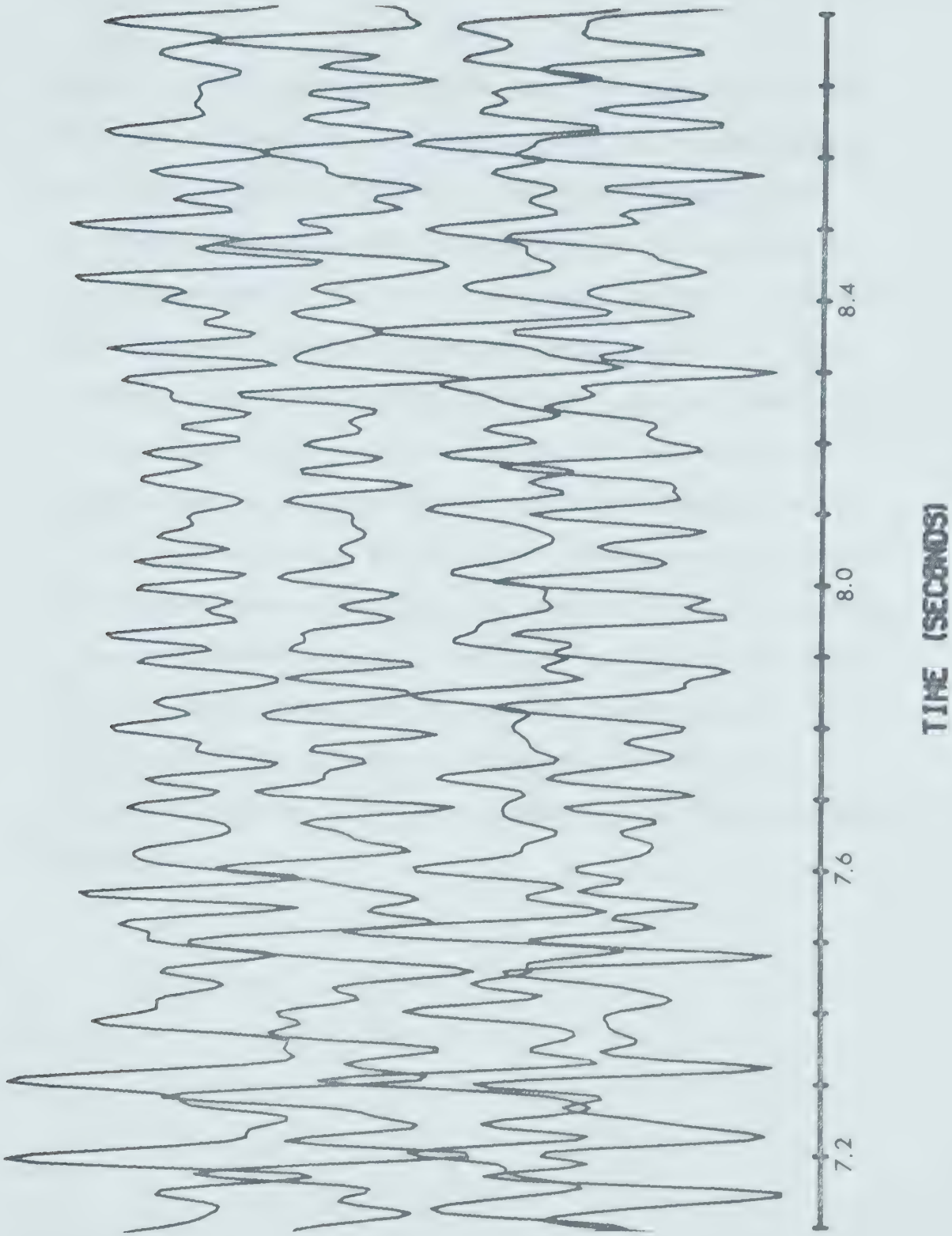

Figure 4.8. Single channel predictive deconvolution. Four channels of data deconvolved by single channel prediction with prediction distance $\alpha = 1$ and $\alpha+m+1 = 7$.

events running through it than has the single channel output in Figure 4.8, but the similarity between the two plots is quite striking. This may suggest that the method of single channel predictive deconvolution is as effective as the method of multichannel predictive deconvolution in defining major reflections. If this is correct, then the method of single channel predictive deconvolution is the preferable one to use, as it is considerably less expensive in terms of computer costs. In one application of multichannel least-squares inverse filtering of common depth point seismic reflection data, it was concluded that the results were no better than those obtained using single channel least-squares inverse filtering (Davies and Mercado, 1968); that conclusion appears to be in agreement with the conclusion reached here.

BIBLIOGRAPHY

Alpaslan, T., 1968. Spectral Behavior of Short Period Body Waves and the Synthesis of Crustal Structure in Western Canada, M.Sc. thesis, Edmonton: University of Alberta, Department of Physics.

Allsopp, D.F., Burke, M.D., and Cumming, G.L., 1972. A Digital Seismic Recording System, Bulletin of the Seismological Society of America, Vol. 62, pp. 1641-1647.

Chandra, N.N., and Cumming, G.L., 1972. Seismic Refraction Studies in Western Canada, Canadian Journal of Earth Sciences, Vol. 9, pp. 1099-1109.

Clowes, R.M., 1966. Deep Crustal Seismic Reflections at Near-Vertical Incidence, M.Sc. thesis, Edmonton: University of Alberta, Department of Physics.

Clowes, R.M., 1969. Seismic Reflection Investigations of Crustal Structure in Southern Alberta, Ph.D. thesis, Edmonton: University of Alberta, Department of Physics.

Clowes, R.M., and Kanasewich, E.R., 1970. Seismic Attenuation and the Nature of Reflecting Horizons within the Crust, Journal of Geophysical Research, Vol. 75, pp. 6693-6705.

Clowes, R.M., Kanasewich, E.R., and Cumming, G.L., 1968. Deep Crustal Seismic Reflections at Near-Vertical Incidence, Geophysics, Vol. 33, pp. 441-451.

Cumming, G.L., Garland, G.D., and Vozoff, K., 1962. Seismological Measurements in Southern Alberta, Final Report, Contract AF 19(604)-8470, Project Vela-Uniform, Air Force Cambridge Research Laboratories, Bedford, Massachussetts.

Cumming, G.L., and Kanasewich, E.R., 1966. Crustal Structure in Western Canada, Final Report, Contract AF 19(628)-2835, Project Vela-Uniform, Air Force Cambridge Research Laboratories, Bedford, Massachusetts.

Davies, E.B., and Mercado, E.J., 1968. Multichannel Deconvolution Filtering of Field Recorded Seismic Data, Geophysics, Vol. 33, pp. 711-722.

Dohr, G., and Fuchs, K., 1967. Statistical Evaluation of Deep Crustal Reflections in Germany, Geophysics, Vol. 32, pp. 951-967.

Ellis, R.M., and Basham, P.W., 1968. Crustal Characteristics from Short Period P Waves, Bulletin of the Seismological Society of America, Vol. 58, pp. 1681-1700.

Fuchs, K., 1969. On the Properties of Deep Crustal Reflectors, Zeitschrift für Geophysik, Vol. 35, pp. 133-149.

Ganley, D.C., 1973. A Seismic Reflection Crustal Model Near Edmonton, Alberta, M.Sc. thesis, Edmonton: University of Alberta, Department of Physics.

Hart, P.J., ed., 1969. The Earth's Crust and Upper Mantle, Geophysical Monograph Series: American Geophysical Union, Washington, D.C.

Heacock, J.G., ed., 1971. The Structure and Physical Properties of the Earth's Crust, Geophysical Monograph Series: American Geophysical Union, Washington, D.C.

Hron, F., 1971. Criteria for Selection of Phases in Synthetic Seismograms for Layered Media, Bulletin of the Seismological Society of America, Vol. 61, pp. 765-779.

Hron, F., and Kanasewich, E.R., 1971. Synthetic Seismograms for Deep Seismic Sounding Studies Using Asymptotic Ray Theory, Bulletin of the Seismological Society of America, Vol. 61, pp. 1169-1200.

Junger, A., 1951. Deep Basement Reflections in Big Horn County, Montana, Geophysics, Vol. 16, pp. 499-510.

Kanasewich, E.R., 1973. Time Sequence Analysis in Geophysics, Edmonton: The University of Alberta Press.

Kanasewich, E.R., and Cumming, G.L., 1965. Near-Vertical-Incidence Seismic Reflections from the 'Conrad' Discontinuity, Journal of Geophysical Research, Vol. 70, pp. 3441-3446.

Knopoff, L., Drake, C.L., and Hart, P.J., eds., 1968. The Crust and Upper Mantle of the Pacific Area, Geophysical Monograph Series: American Geophysical Union, Washington, D.C.

McDonal, F.J., Angona, F.A., Mills, R.L., Sengbush, R.L., Van Nostrand, R.G., and White, J.E., 1958. Attenuation of Shear and Compressional Waves in Pierre Shale, Geophysics, Vol. 23, pp. 421-439.

Meisner, R., 1967. Exploring Deep Interfaces by Seismic Wide-angle Measurements, Geophysical Prospecting, Vol. 15, pp. 598-617.

O'Brien, P.N.S., 1969. Some Experiments Concerning the Primary Seismic Pulse, Geophysical Prospecting, Vol. 17, pp.511-547.

Peacock, K.L., and Treitel, S., 1969. Predictive Deconvolution: Theory and Practice, Geophysics, Vol. 34, pp. 155-169.

Richards, T.C., and Walker, D.J., 1959. Measurement of the Thickness of the Earth's Crust in the Albertan Plains of Western Canada, Geophysics, Vol. 24, pp. 262-284.

Robinson, E.A., 1954. Predictive Decomposition of Time Series with Application to Seismic Exploration, Ph.D. thesis, Cambridge: Massachusetts Institute of Technology, Department of Mathematics. Reprinted in Geophysics, Vol. 32, pp. 418-484.

Robinson, E.A., 1964. Wavelet Composition of Time Series, and Recursive Decomposition of Stochastic Processes, In Econometric Model Building: Essays on the Causal Chain Approach, Wold, H.O.A., ed., Amsterdam: North-Holland Publishing Company.

Robinson, E.A., 1966. Collection of Fortran II Programs for Filtering and Spectral Analysis of Single Channel Time Series, Geophysical Prospecting, Vol. 14, Supplement.

Robinson, E.A., 1967. Multichannel Time Series Analysis with Digital Computer Programs, San Francisco: Holden-Day, Inc.

Schriever, W., 1952. Reflection Seismograph Prospecting - How It Started, Geophysics, Vol. 17, pp. 936-942.

Somerville, P.G., and Ellis, R.M., 1972. P-Coda Evidence for a Layer of Anomalous Velocity in the Crust Beneath Leduc, Alberta, Canadian Journal of Earth Sciences, Vol. 9, pp. 845-856.

Sprenke, K.F., 1972. An Application of the P-Coda Spectral Ratio Method to Crustal Structure in Central Alberta, M.Sc. thesis, Edmonton: University of Alberta, Department of Physics.

Steinhart, J.S., and Meyer, R.P., 1961. Explosion Studies of Continental Structure, Carnegie Institute of Washington Publication 622, Washington, District of Columbia.

Steinhart, J.S., and Smith, T.J., eds., 1966. The Earth Beneath the Continents, Geophysical Monograph Series: American Geophysical Union, Washington, D.C.

Vogel, A., ed., 1971. Proceedings of the Colloquium on Deep Seismic Sounding in Northern Europe held in Uppsala on December 1 and 2, 1969, The Swedish Natural Science Research Council (NFR), Stockholm, 1971.

Wiggins, R.A., and Robinson, E.A., 1965. Recursive Solution to the Multichannel Filtering Problem, Journal of Geophysical Research, Vol. 70, pp. 1885-1891.

APPENDIX

TRANSFER FUNCTIONS OF THE SEISMIC RECORDING INSTRUMENTS AND SEISMOMETERS

In order to obtain the s-plane representation of the seismic recording instruments and seismometers, it is necessary to find an expression for each of the instruments. In the following paragraphs, the s-plane representation of the seismometers is derived.

Each seismometer consists of a frame in which a mass m is suspended vertically by a spring with spring constant k and the motion of the mass is damped by a force proportional to velocity with damping constant α. If y represents the upward displacement of the frame, and q represents the upward displacement of the mass, let x be defined as the relative upward displacement of the frame and mass,

$$x = y - q \quad . \tag{A.1}$$

At equilibrium,

$$mg = kl \quad , \tag{A.2}$$

where g is the acceleration of gravity and l is the extension of the spring. If the seismometer frame moves y and the mass moves q, the equation of motion is

$$k(l + y - q) + \alpha(\dot{y} - \dot{q}) - mg = m\ddot{q} \quad . \qquad \text{A.3}$$

Using equation A.2, equation A.3 becomes

$$k(y - q) + \alpha(\dot{y} - \dot{q}) = m\ddot{q} \quad . \qquad \text{A.4}$$

Now, using equation A.1, equation A.4 becomes

$$kx + \alpha\dot{x} = m(\ddot{y} - \ddot{x}) \quad , \qquad \text{A.5}$$

or

$$kx + \alpha\dot{x} + m\ddot{x} = m\ddot{y} \quad . \qquad \text{A.6}$$

If the right-hand side is set equal to zero, the characteristic equation is obtained,

$$kx + \alpha\dot{x} + m\ddot{x} = 0 \quad . \qquad \text{A.7}$$

If there is no damping, $\alpha = 0$, and the solution of equation A.7 is sinusoidal motion with a natural frequency

$$\omega_n = \sqrt{k/m} \quad . \qquad \text{A.8}$$

Thus, equation A.6 may be written

$$x + \frac{\alpha}{m\omega_n^2}\dot{x} + \frac{1}{\omega_n^2}\ddot{x} = \frac{1}{\omega_n^2}\ddot{y} \quad . \qquad \text{A.9}$$

If the Laplace transform of each side of equation A.9 is taken, equation A.9 becomes

$$X(s) + \frac{\alpha s}{m\omega_n^2} X(s) + \frac{s^2}{\omega_n^2} X(s) = \frac{s^2}{\omega_n^2} Y(s) \quad . \qquad \text{A.10}$$

Now, define a normalized complex frequency

$$S = \frac{s}{\omega_n} = \frac{\sigma + i\omega}{\omega_n} \quad ; \qquad \text{A.11}$$

then equation A.10 becomes

$$X(S)\left[1 + \frac{\alpha}{m\omega_n} S + S^2\right] = S^2 Y(S) \quad . \qquad \text{A.12}$$

The transfer function in S of output displacement for an input delta function in displacement is defined as

$$T_d(S) = \frac{X(S)}{Y(S)} = \frac{S^2}{1 + \frac{\alpha}{m\omega_n} S + S^2} \quad . \qquad \text{A.13}$$

The output voltage is proportional to the velocity and is given by

$$e(x) = -G\dot{x} \quad ; \qquad \text{A.14}$$

taking the Laplace transform of each side of equation A.14 gives

$$E(s) = -G\, s\, X(s) \quad , \qquad \text{A.15}$$

or, in terms of the normalized complex frequency S,

$$E(S) = -G\omega_n S\, X(S) \quad . \qquad \text{A.16}$$

The transfer function in S of output voltage for an input delta function in displacement is, therefore,

$$T_v(S) = \frac{E(S)}{Y(S)} = \frac{-G\omega_n S^3}{1 + \frac{\alpha S}{m\omega_n} + S^2} \quad . \qquad \text{A.17}$$

The transfer function in S of an n-pole low pass filter is

$$T_L(S) = \frac{1}{F_0 + F_1 S + F_2 S^2 + \ldots + F_n S^n} \quad , \qquad \text{A.18}$$

and the transfer function in S of an n-pole high pass filter is

$$T_H(S) = \frac{S^n}{F_0 + F_1 S + F_2 S^2 + \ldots + F_n S^n} \quad , \qquad \text{A.19}$$

where $F_0, F_1, F_2, \ldots, F_n$ are constants which describe the filter. A bandpass filter has a transfer function in S which is the product of the transfer function in S of a low pass filter and the transfer function in S of a high pass filter.

The constants in the s-plane representations of the seismic recording instruments and seismometers may be found by examining the specifications of the circuits and their components. Then, these nominal values may be adjusted slightly so that the amplitude and phase

spectra calculated from the specifications match the amplitude and phase spectra determined experimentally. The constants in the s-plane representations of the seismic recording instruments and seismometers were determined according to this procedure by Cumming.

In the following paragraphs, the parameter S equals $i\omega/2\pi$. The function subprogram which expresses the s-plane transfer function of the seismic recording instruments used at the University of Alberta in 1969 follows:

```
  COMPLEX FUNCTION TRANS(S)
  COMPLEX S
  TRANS=
 1((S/.10)/(1.0+S/.10))*1.0/(1.0+1.2*S/4700.+(S/4700.)**2)
C THE TRANSFORMER
 1*(S/.130)/(1.0+S/.130)
C THE GAIN CONTROL OF THE PREAMP -- NOMINAL IS .120
 1*(S/.169)/(1.0+S/.169)
C THE SECOND GAIN CONTROL
 1*(S/.311)/(1.0+S/.311)
 1*(S/.329)/(1.0+S/.329)
 1*((S/.333)/(1.0+S/.333))**2
C THE LOW CUT FILTERS
 1*(1.0/(1.0+S/57.3))**4
C HIGH CUT FILTERS -- NOMINAL VALUE OF 52.1 HZ. INCREASED
C BY 10%
 1*(S/.600)/(1.0+S/.600)
C THE OUTPUT TO F.M. TAPE -- NOMINAL IS .455 HZ.
  RETURN
  END
```

The function subprogram which expresses the s-plane transfer function of the seismic recording instruments used at the University of Alberta in 1970 follows:

```
      COMPLEX FUNCTION TRANS(S)
      COMPLEX S
      TRANS=
     1((S/.10)/(1.0+S/.10))*1.0/(1.0+1.2*S/4700.+(S/4700.)**2)
C THE TRANSFORMER
     1*(S/.120)/(1.0+S/.120)
C THE GAIN CONTROL OF THE PREAMP
     1*(S/.169)/(1.0+S/.169)
C THE SECOND GAIN CONTROL
     1*(S/.311)/(1.0+S/.311)
     1*(S/.329)/(1.0+S/.329)
     1*((S/.333)/(1.0+S/.333))**2
C THE LOW CUT FILTERS
     1*(1.0/(1.0+S/46.0))**4
C THE HIGH CUT FILTERS -- NOMINAL VALUE IS 52.1 HZ.
     1*(S/.260)/(1.0+S/.260)
C THE OUTPUT STAGE
      RETURN
      END
```

The function subprogram which expresses the s-plane transfer function of the seismic recording instruments and seismometers used at the University of Alberta in 1971 follows:

```
      COMPLEX FUNCTION TRANS(S)
      COMPLEX S
      TRANS=
     1((S/.10)/(1.0+S/.10))*1.0/(1.0+1.2*S/4700.+(S/4700.)**2)
C THE TRANSFORMER
     1*1.0/(1.0+S/53.1)
C THE PREAMPLIFIER
     1*(S/.100)/(1.0+S/.100)
C THE D.C. OFFSET FILTER
     1*1.0/(1.0+S/53.1)
C THE GAIN CONTROL
     1*105./(105.+105.*2.1105*S/50.+45.*(2.1105*S/50.)**2
     1+10.*(2.1105*S/50.)**3+(2.1105*S/50.))**4)
C THE FOUR POLE BESSEL FILTER WITH A FUDGE FACTOR FOR
C FREQUENCY
     1*(S/7.5)**2/(1.0+1.4*S/7.5+(S/7.5)**2)
C THE SEISMOMETERS
      RETURN
      END
```

If the fourth last line of the subprogram and its corresponding comment card are omitted, the function subprogram which expresses the s-plane transfer function of the seismic recording instruments used at the University of Alberta in 1971 is obtained.

Figure A.1 shows the amplitude and phase spectra, determined from the transfer function, of the seismic recording instruments used at the University of Alberta in 1969. In Figures A.1, A.2, A.3, and A.4, frequency is on a logarithmic scale, ranging from one-hundredth to one hundred Hertz, while amplitude, or gain, is in decibels and phase is in degrees. Figures A.2, A.3, and A.4 show the amplitude and phase spectra, determined from the transfer functions, of the seismic recording instruments used at the University of Alberta in 1970, of the seismic recording instruments used at the University of Alberta in 1971, and of the seismic recording instruments and seismometers used at the University of Alberta in 1971, respectively.

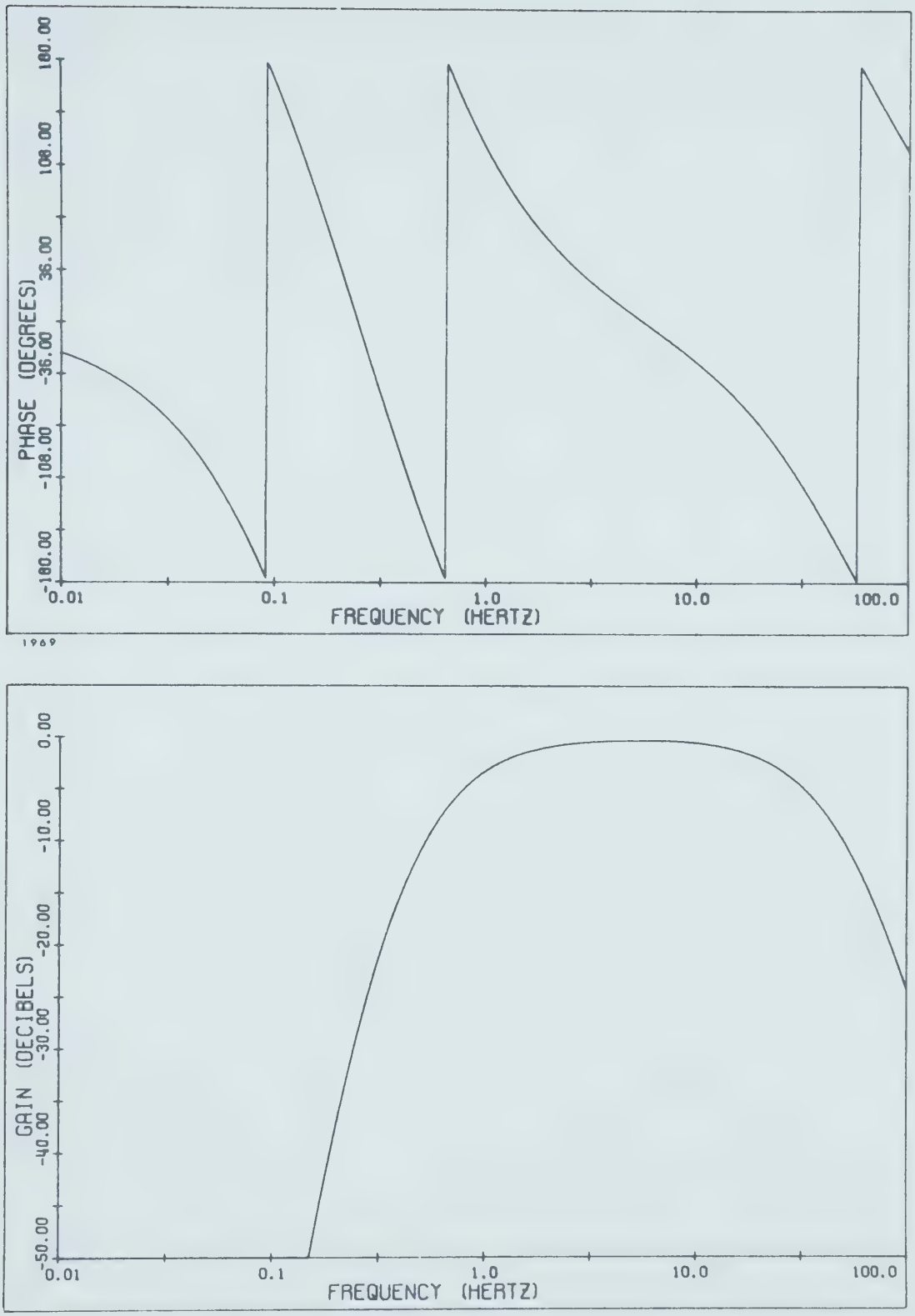

Figure A.1. Amplitude and phase spectra of the seismic recording instruments used at the University of Alberta in 1969.

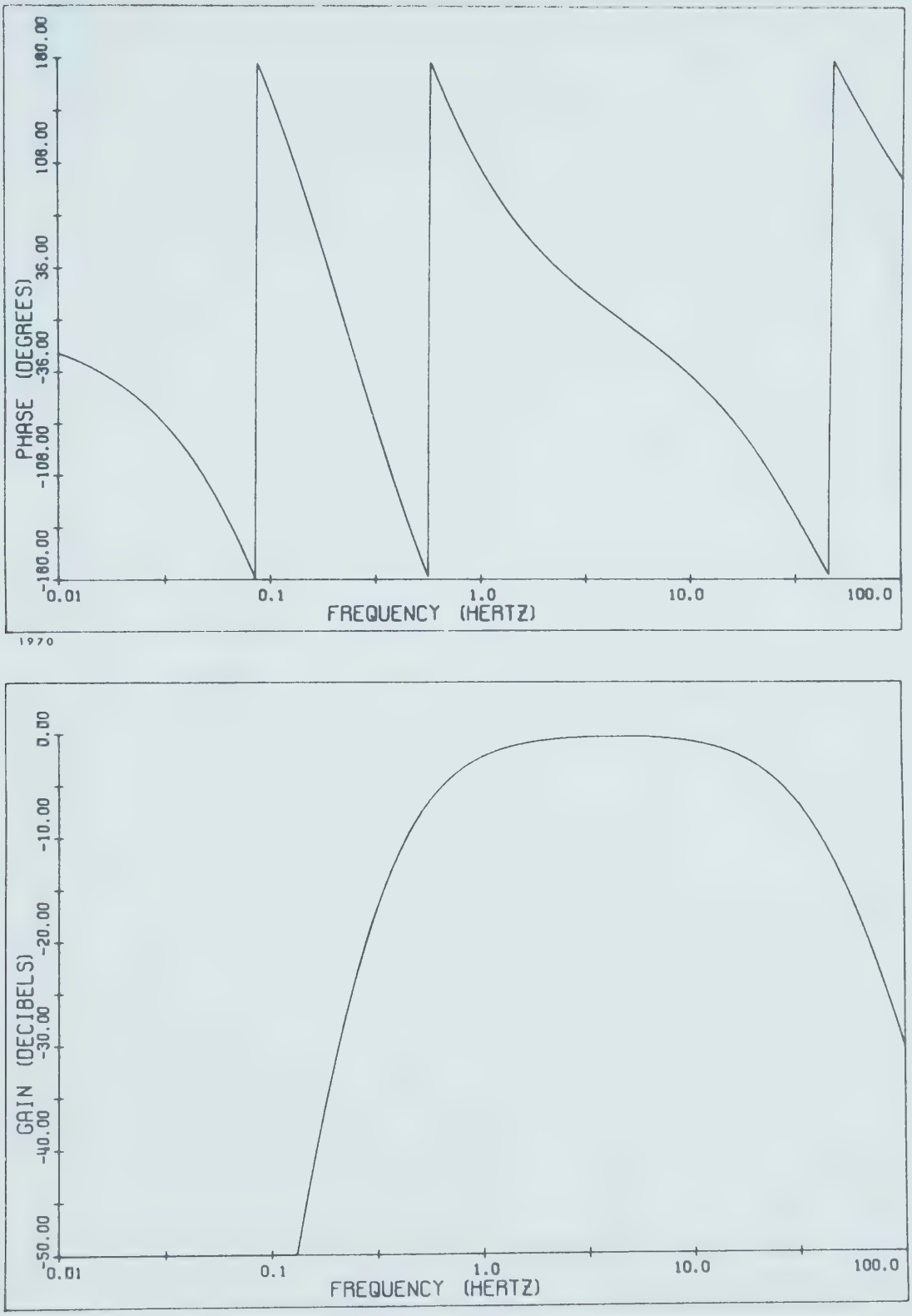

Figure A.2. Amplitude and phase spectra of the seismic recording instruments used at the University of Alberta in 1970.

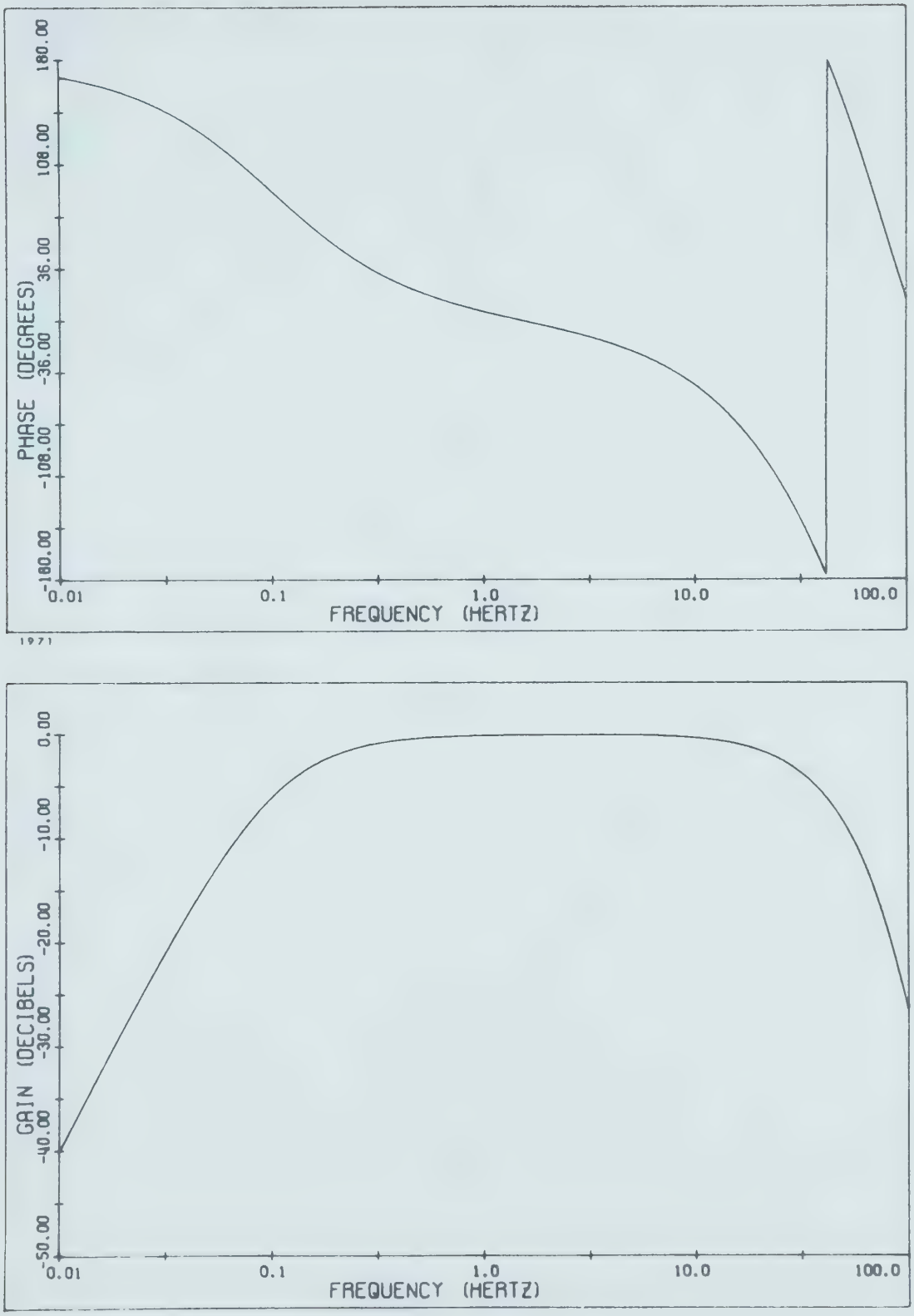

Figure A.3. Amplitude and phase spectra of the seismic recording instruments used at the University of Alberta in 1971.

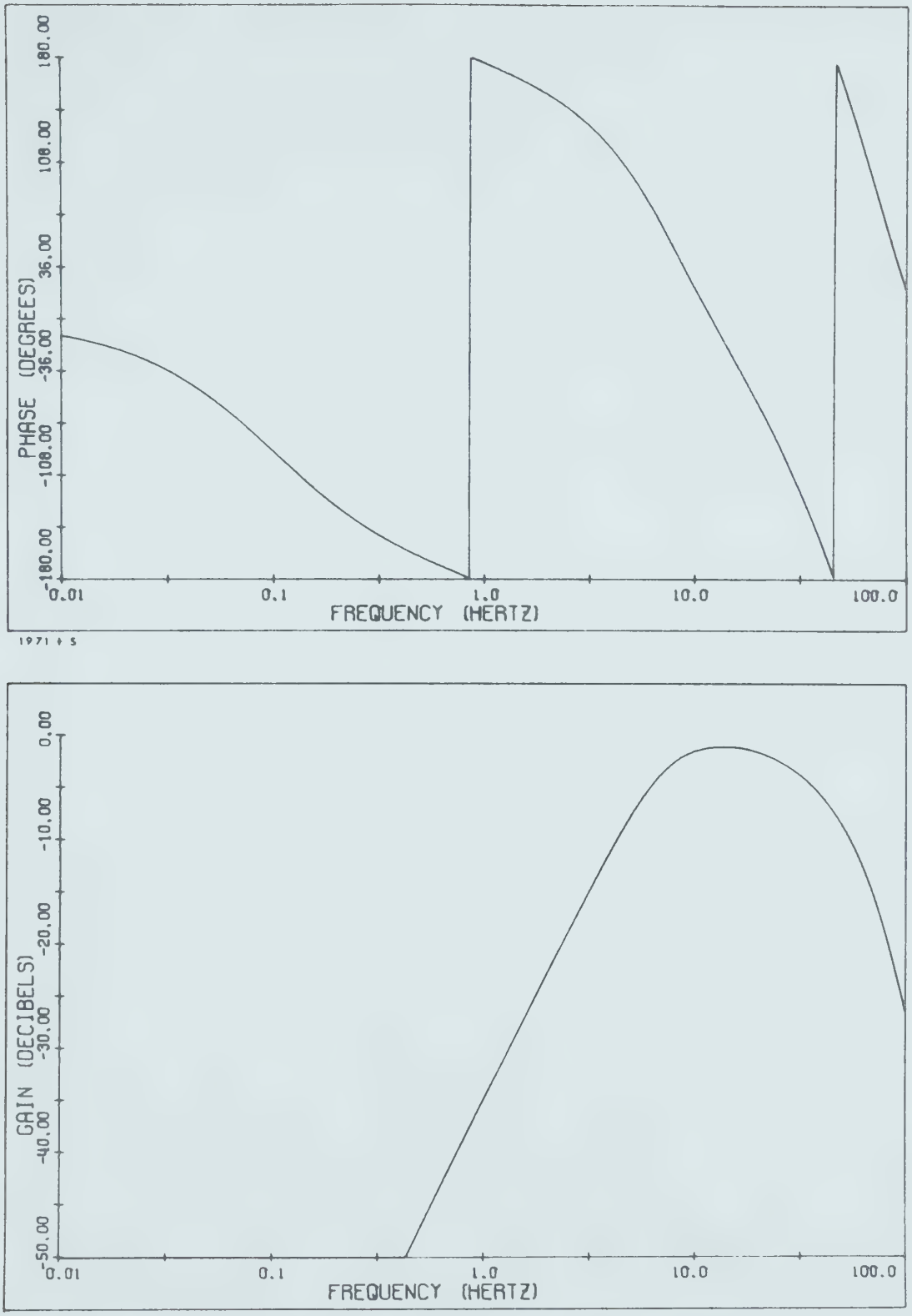

Figure A.4. Amplitude and phase spectra of the seismic recording instruments and seismometers used at the University of Alberta in 1971.